FACIAL SOFT TISSUE SEGMENTATION IN MRI USING UNLABELED ATLAS

A THESIS SUBMITTED TO
THE GRADUATE SCHOOL OF NATURAL AND APPLIED SCIENCES
OF
MIDDLE EAST TECHNICAL UNIVERSITY

BY

YOUSEF REZAEITABAR

IN PARTIAL FULFILLMENT OF THE REQUIREMENTS
FOR
THE DEGREE OF MASTER OF SCIENCE
IN
BIOMEDICAL ENGINEERING

AUGUST 2011

Approval of the thesis:

FACIAL SOFT TISSUE SEGMENTATION IN MRI USING UNLABELED ATLAS

Submitted by **YOUSEF REZAEITABAR** in partial fulfillment of the requirements for the degree of **Master of Science in Biomedical Engineering Department, Middle East Technical University** by,

Prof. Dr. Canan Özgen _____
Dean, Graduate School of **Natural and Applied Sciences**

Prof. Dr. Semra Kocabıyık _____
Head of Department, **Biomedical Engineering**

Asst. Prof. Dr. Ilkay Ulusoy _____
Supervisor, **Electrical and Electronics Engineering Dept., METU**

Assoc. Prof. Dr. Özlem Üçok _____
Co-Supervisor, **Gulhane Military Medical Academy**

Examining Committee Members:

Prof. Dr. Nevzat Güneri Gençer _____
Electrical and Electronics Engineering Dept., METU

Asst. Prof. Dr. Ilkay Ulusoy _____
Electrical and Electronics Engineering Dept., METU

Asst. Prof. Dr. Yeşim Serinağaoğlu Doğrusöz _____
Electrical and Electronics Engineering Dept., METU

Assist. Prof. Dr. Didem Gökçay _____
Informatics Institute, METU

Prof. Dr. Ergin Atalar _____
Electrical and Electronics Engineering Dept., Bilkent University

Date: _____

I hereby declare that all information in this document has been obtained and presented in accordance with academic rules and ethical conduct. I also declare that, as required by these rules and conduct, I have fully cited and referenced all material and results that are not original to this work.

Name, Last name : Yousef Rezaeitabar

Signature :

ABSTRACT

FACIAL SOFT TISSUE SEGMENTATION IN MRI USING UNLABELED ATLAS

Rezaeitabar,Yousef

M.Sc., Department of Biomedical Engineering
Supervisor: Assist. Prof. Dr. Ilkay Ulusoy
Co-Supervisor: Assoc. Prof. Dr. Özlem Üçok

August 2011, 98 pages

Segmentation of individual facial soft tissues has received relatively little attention in the literature due to the complicated structures of these tissues. There is a need to incorporate the prior information, which is usually in the form of atlases, in the segmentation process. In this thesis we performed several segmentation methods that take advantage of prior knowledge for facial soft tissue segmentation. An atlas based method and three expectation maximization – Markov random field (EM-MRF) based methods are tested for two dimensional (2D) segmentation of masseter muscle in the face. Atlas based method uses the manually labeled atlases as prior information. We implemented EM-MRF based method in different manners; without prior information, with prior information for initialization and with using labeled atlas as prior information. The differences between these methods and the influence of the prior information are discussed by comparing the results. Finally a new method based on EM-MRF is proposed in this study. In this method we aim to use prior information without performing manual segmentation, which is a very complicated and time consuming task.

10 MRI sets are used as experimental data in this study and leave-one-out technique is used to perform segmentation for all sets. The test data is modeled as a Markov Random Field where unlabeled training data, i.e., other 9 sets, are used as prior information. The model parameters are estimated by the Maximum Likelihood approach when the Expectation Maximization iterations are used to handle hidden labels. The performance of all segmentation methods are computed and compared to the manual segmented ground truth. Then we used the new 2D segmentation method for three dimensional (3D) segmentation of two masseter and two temporalis tissues in each data set and visualize the segmented tissue volumes.

Keywords: Facial soft tissue, segmentation, prior information, Markov random field, atlas, unlabelled atlas

ÖZ

YÜZ BÖLGESİ YUMUŞAK DOKUSUNUN ATLAS TEMELLİ SEGMENTASYONU

Rezaeitabar,Yousef

Yüksek Lisans, Biyomedikal Mühendisliği Anabilim Dalı
Tez Yöneticisi: Yrd. Doç. Dr. Ilkay Ulusoy
Ortak Tez Yöneticisi: Doç. Dr. Özlem Üçok
Ağustos 2011 , 98 sayfa

Yumuşak yüz dokularının tek tek bölütlenmesi işi, bu dokuların karmaşık yapıları yüzünden, ilgili diğer konularla karşılaştırılacak olursa, literatürde şimdiye kadar pek rağbet görmemiş konulardan birisidir. Bu tek tek bölütleme işini başarmak için, genellikle atlas formunda bulunan ön bilgileri bölütleme safhasına katmak bir gereksinim olarak karşımıza çıkmaktadır. Bu yüzden, bu tezde, öncelikle, yumuşak yüz dokuları hakkındaki ön bilgilerden faydalanan birtakım bölütleme yöntemleri uygulanmaktadır. Bu yöntemler, atlaslara dayanan bir metod ve EM-MRF'e dayanan bir metodun üç farklı şekilde uygulanmasından oluşmaktadır ve bu metodlar, performans ölçümü için, yüzdeki çiğneme(masseter) kasının iki boyutlu bölütlenmesinde test edilmektedir. Atlaslara dayanan ilk metod, ön bilgi olarak elle işaretlenmiş atlasları kullanmaktadır. Diğer bir yandan, EM-MRF'e dayanan metod, az önce bahsedildiği gibi üç farklı biçimde uygulanmaktadır: ön bilgi kullanmadan, sadece başlangıç için ön bilgi kullanarak ve ön bilgi olarak işaretlenmiş atlasları kullanarak. Testlerden sonra, tüm bu yöntemlerin sonuçları birbiriyle

karşılaştırılmakta ve sonuçlar arasındaki farklar ile ön bilgilerin bu sonuçlara etkisi tartışılmaktadır. Daha sonra, bu tezde, EM-MRF'e dayanan yeni bir metod önerilmektedir. Bu metodun amacı, bölütleme işini, çokça karmaşık olan ve oldukça zaman alan elle işaretlemeyi kullanmadan yaratılan ön bilgiyi kullanarak başarmaktır.

Bu çalışmada, deneysel veri olarak 10 MRI seti kullanılmaktadır. Her bir setin bölütlenmesi, sadece, o seti, eğitim verisi dışında bırakarak gerçekleştirilmektedir. Test verisi, Markov Rassal Alanlar(Markov Random Field) olarak modellenmekte ve geriye kalan etiketlenmemis 9 setten oluşan eğitim verisi, ön bilgi olarak kullanılmaktadır. Modelin parametreleri, Azami Olabilirlik (Maximum Likelihood) yaklaşımı ile hesaplanmakta ve yinelemelei beklenti en iyilestirme ile gizli etiketler incelenmektedir.. Uygun parametreler bulunduktan sonra, bahsedilen tüm bölütleme algoritmalarının performansları hesaplanmakta ve bu performanslar, elle işaretlenmiş kesin referans(ground truth) ile karşılaştırılmaktadır. Daha sonrasında, bu tezde önerilen yeni iki boyutlu bölütleme yöntemi, her veri setindeki iki adet çiğneme(masseter) ve iki adet şakak atardamarı(temporalis) dokusunun üç boyutlu bölütlenmesinde kullanılmakta ve bölütlenmiş doku kısımları gösterilmektedir.

Anahtar Sözcükler: Yumuşak yüz dokuları, ön bilgi, Markov Rassal Alanlar, atlas, işaretlenmemiş atlas

To My Family,

ACKNOWLEDGMENTS

I would like to express my sincere gratitude and appreciation to my supervisor Asst. Prof. Dr. Ilkay Ulusoy for her endless support throughout this research. She was always an advisor, professor, and personal friend for me during my master's period.

I would like to thank Assoc. Prof. Dr. Özlem Üçok who gave me invaluable suggestions about my thesis.

I would like to thank my friend Örsan Aytekin whose suggestions and encouragement helped me a lot during my study. I also wish to thank my friend Ceren Bora for her friendly guidance throughout my thesis.

Finally, I would like to express my special thanks to my parents for their love and support during my education.

TABLE OF CONTENTS

LIST OF TABLES

TABLES

LIST OF FIGURES

FIGURES

CHAPTER 1

INTRODUCTION

1.1. Motivation of the Thesis

Recent advances in medical imaging have enabled the derivation of useful information about different body parts and tissues. As two major imaging modalities, Computed Tomography (CT) and Magnetic Resonance Imaging (MRI) are commonly used as a source to extract anatomical structures. Despite CT scans specialize in hard tissues, such as bone, MR images are well known for good quality in soft tissues. Magnetic resonance imaging is a commonly preferred source of data for evaluating the presence and extent of the soft tissue volumes such as brain, heart, etc.

Nowadays doctors and clinical specialists take the advantage of these imaging modalities in gathering anatomical information about a patient and are able to use this information in diagnosis and prognosis. The further step is to involve artificial intelligence to automate this diagnosis/ prognosis process. In order to be able to use medical images in an automatic clinical system, the first thing that should be done is to segment target tissues which means that the structure of the target tissue should be extracted in the whole image.

Currently, there are many researches that perform segmentation in medical images. Most of the soft tissue segmentation methods in the literature consider tissues like brain, heart and lung as target tissues and there are very few works about Facial Soft Tissue (FST) segmentation. Considering the key role of the face in

human life and the huge increase in craniofacial surgeries around the world, FST segmentation has become more important in recent days.

Planning before a facial surgery by performing the modifications virtually prior to the actual operation is very important to increase the overall success of the actual operation. Also, for patients seeking for surgical treatment, it would be very beneficial to have a means to predict the post-surgical appearance of their face. For these to be done, the first step is to obtain an anatomic model of the patient's face. Such a complicated computer model should include segmented hard (i.e. skull) and soft tissues (i.e, muscles, skin and fat). Besides, each FST (e.g, a muscle) should also be segmented from the others when the operation has an effect on such a tissue. Only then, the operation can be planned realistically and even simulated on the computer model before the actual operation.

1.2. Scope of the Thesis

In this thesis, we test the accuracy of several state of art methods for FST segmentation and propose a new method for this purpose which requires very little user interaction. Soft tissue segmentation is very complicated due to the fact that soft tissues do not have a constant shape. Moreover, segmentation becomes more complicated when the soft tissues interfere with each other and this is always the case for FSTs. Thus, most of the soft tissue segmentation methods are not appropriate for FST segmentation.

To solve these problems, additional information is needed besides image intensities. Prior information is commonly used in different manners to improve segmentation quality.

By prior information, we mean the knowledge that we take from different individual MRI scans which can be used to determine prior shapes and locations of the target tissues. This is quite like the method when a specialist doctor extracts the target tissue in a new image based on his/her past experience of viewing thousands of similar images. The prior information is usually incorporated in the form of atlases, where information from many manually segmented data sets is combined to

construct a deterministic or probabilistic atlas. The atlas can be used in several manners. The standard atlas based segmentation method is to register the labeled atlas to the test MRI set and apply the labeling to the test set based on the transformation in the registration process. The atlas can also be used as the prior labeling information in a Markov Random Field (MRF) statistical model to optimize the segmentation.

Currently these methods are tested for tissues other than FST but we employed these methods to segment several facial soft tissues for the first time. We implemented representative examples of the methods in the literature and compared them for the purpose of segmentation of four different FSTs (left masseter, right masseter, left temporalis and right temporalis). Also, we proposed a new method, which is very different from all these previous approaches, to perform 3D segmentation on these four tissues. Our method is also MRF based but we did not use manually labeled atlases but, instead, we used unlabeled images as hidden atlases for the purpose of evaluating the effect of unlabeled prior information. The main reason in using the unlabeled prior information is that manual labeling of tens of medical image data sets is a very complicated and time consuming task and is prone to error.

Different from the previous approaches, the prior knowledge was used in our MRF structure via a novel energy function and we tried to optimize the segmentation results iteratively by using Expectation Maximization (EM) algorithm. Finally, we compared our segmentation method with the previously mentioned segmentation methods and evaluate the advantages and disadvantages of each of the methods.

1.3. Thesis Outline

This Thesis is organized as follows: In the 1st chapter the scope and motivation of the thesis are introduced. A survey of current studies in medical image segmentation fields is presented in the 2nd chapter. In the 3rd chapter theoretical aspects of the thesis are explained and the mathematical solutions for the problem

are presented. In the 4th chapter, used datasets, segmentation algorithms and the implementation of each method are explained. The performance evaluation of the presented methods is presented in chapter 5.

Finally, the overall conclusion of the research and the potential future work are described in chapter 6.

CHAPTER 2

LITERATURE SURVEY

2.1. Soft Tissue Segmentation

Today, medical imaging technologies have greatly increased knowledge of normal and diseased anatomy of tissues so that this information serves as the basis for medical diagnosis and prognosis. These imaging modalities provide specialized image data that can be used in different aspects of medical research and clinical applications. Common imaging techniques include X-RAY, Computed Tomography (CT), Ultrasound and Magnetic resonance imaging (MRI). CT and MRI are most preferred imaging modalities in anatomical researches because they provide three-dimensional (3D) data with high contrast. CT is a sophisticated form of X-ray imaging that provides clear shape information about hard tissues. MRI, on the other hand, is a non-invasive imaging technique that provides high spatial resolution and contrast of human soft tissue anatomy. However, since the amount of data is too much for manual analysis (such as segmentation), automatic or semi-automatic techniques of computer-aided image analysis are necessary.

Tissue segmentation in MRI scans is a method to extract structural information from the image data. Automatic segmentation of tissues can help clinical specialists detect the human body parts fast and precisely. The segmented data compared with a database of previously segmented images can also help doctors in detecting any tissue disorders. Different segmentation methods are

applied to medical images due to the variations in tissue types and desired objectives. These methods mainly target important soft tissues in human body such as brain and heart.

Because of the critical role of human face, morphological information about human Facial Soft Tissues (FST) like muscles and fats has a great importance. Once the structural shape of target facial tissues are segmented successfully, the resulting model can be used in several medical fields like diagnosis of craniofacial disorders [1], the planning of computer assisted surgery (CASP) [2]and the prediction of post-operative facial appearance [3].

Although there are plenty of methods that perform soft tissue segmentation in the literature, Facial Soft Tissue (FST) segmentation has received relatively little attention. Considering the visualization similarities between FST and other soft tissues like brain, the segmentation process can be the same theoretically but due to different characteristics of these tissues, such as more complicated and interfered structure of FSTs, they need more precise and powerful segmentation methods.

Facial soft tissues are usually small and surrounded with other tissues that share the same intensity values with them [1]. Different but neighboring tissues are interfering with each other in some cases that makes tissue detection a hard work even for a specialist doctor. Other than that, unlike other tissues like brain that have a specific shape model, FSTs do not have a specific shape but they may have different shapes in different individuals. All these difficulties make the segmentation process a hard work and thus the requirement of additional information is inevitable.

In this chapter, we will discuss soft tissue segmentation studies that are related to our work and we also try to cover all segmentation methods that can be applied to FSTs. There are plenty of methods to segment an image, that is, to assign an appropriate label to each of its pixels or voxels. For different type of image modalities and targets, different kinds of segmentation methods should be applied. Simple segmentation methods like thresholding [4] or region growing are usually inefficient in medical image segmentation. Instead, improved state of art

segmentation methods are applied. Fuzzy clustering algorithms [5] group the image based on intensity similarities between the images.

Standard fuzzy c-means method is not very successful in medical images because of the amount of noise present especially in soft tissue MR images. New studies apply some modifications to the standard methods mentioned above to deal with this problem. In, [6] a fuzzy c-means algorithm is applied for brain MRI segmentation. The objective function of the standard c-means algorithm is modified with weighted bias estimation to decrease the effect of intensity inhomogeneties in tissues. A new weighting exponent is proposed in [7] for fuzzy c-means algorithm. The method is tested in breast MRI segmentation. The number of clusters has a key role in these kind of clustering methods that makes these methods inefficient for FST segmentation.

In [8], a subject-specific dynamical model (SSDM) is developed to segment the structural shape of the left ventricle. The starting slice is segmented manually and the algorithm proceeds through the slices and applies the segmentation based on the prediction from the previous slice. The main idea of this method is to use the prior information from a set of training shapes. Patterns of variations in shapes and spatial relationships between successive slices of the training shapes are used to perform the segmentation in the target slice.

An unsupervised method for segmentation of MR images is introduced in [9]. The method is based on Maximization of the Evidence (ME). Two different models are examined for brain tissues and the model parameters are estimated using ME algorithm.

These purely intensity-based segmentation and classification methods assign a label to each pixel in the image and require only intensity information that is routinely generated by the MR imaging device. However, in medical image segmentation, different anatomical structures may have the same intensity values or distributions that cannot be distinguished from one another by looking at their intensity values in the image.

In such cases, extra information should be considered and included in the segmentation process. Spatial information like neighborhood relationships between

pixels can be very useful in segmenting individual tissues. In addition to geometrical constraints, relationships between several different but similar data sets can also be considered. The additional data that is used in a segmentation process is called as the prior information. Soft tissue segmentation methods usually use prior information in different manners to improve the segmentation accuracy. The prior information is included mostly in the form of single or multiple atlases. An atlas can be presented as a single manually segmented data (2D image or 3D voxel volume or 2D/3D sequences) or can be formed from multiple manually segmented data [10]. For example, 70 infant brain MRI [11], 275 brain dataset [12] and 14 cardiac image sequences [13] were used to construct atlases.

Atlas can be constructed and used in the segmentation process with four different strategies: segmentation with one single individual atlas, segmentation with varying single individual atlases, segmentation with an average shape atlas, and simultaneous segmentation with multiple atlases [14]. A brief overview of each strategy is shown in Figure 2.1. Several studies show that segmentation methods using multi atlas outperform the ones using single atlas [15-16] .

As the number of atlases fused increases, the average segmentation accuracy increases [15] . Fusion of a large number of atlases is more likely to create a smooth estimate of the structure. However, construction of multi atlas is very hard because it requires manual segmentation on tens of data. In addition, increased computational cost of registering large numbers of atlases to the query image is an immediate practical problem. There are some solutions proposed for this problem in literature. In [16], adaptive multi atlas is proposed where local atlas based operations are performed. The proposed algorithm automatically selects the most appropriate atlases for a target image and automatically stops registering atlases when no further improvement is expected.

Another problem of multiple atlases occurs when structure can have two totally different shapes. When all possibilities are fused, a shape, which is not possible, may result in the final atlas. As a solution to this problem, a suitable atlas among the possible ones is used as the prior information. In [17], an appropriate atlas is selected based on the scale resemblance of the atlas and the query data.

Atlases should be registered to the query data before the segmentation process. Segmentations in atlases are transformed to the query data and subsequently fused or combined. Fusion can be done in various ways which can be categorized into four groups: Simple atlas registration, atlas registration with linear interpolation, atlas registration based on active contours and MRF based methods. Studies related with each method are explained in the following section.

Although atlas based methods proved to be powerful in soft tissue segmentation, making an atlas set that covers all possible shapes is a huge work and needs a lot of manual segmentation.

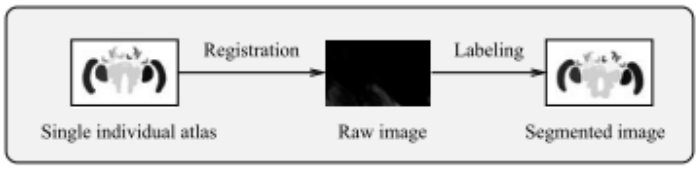

IND: Segmentation using a single individual atlas.

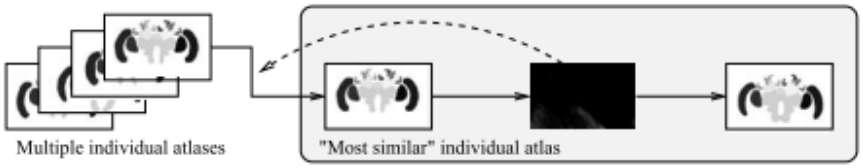

SIM: Segmentation using the “most similar” individual atlas.

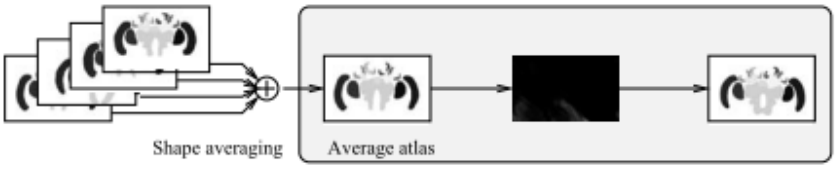

AVG: Segmentation using an average shape atlas.

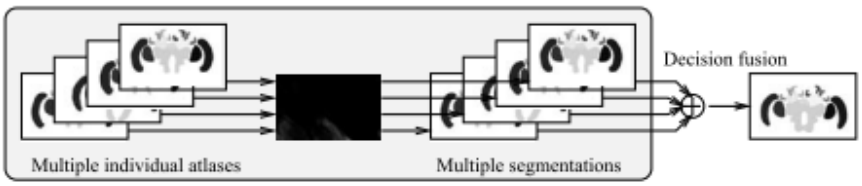

MUL: Independent segmentation using multiple individual atlases with decision fusion.

Figure 2.1 Atlas based segmentation strategies

2.2. Simple atlas registration

One way of atlas registration is to transform the atlas segments to the test data by using nearest neighbor interpolation so that each atlas provides a discrete labeling for each voxel. The final label can then be decided by 'majority vote' [14].

2.3. Atlas registration with linear interpolator

In this method, individual labels are transferred and an array of values for a given voxel is formed as a probabilistic estimate. The array elements represent the confidence levels or probabilities of the possible labels assigned to the voxel at the current segmentation step. Then, different rules can be used to generate a consensus estimate among the array elements.

In [18], the prior information is represented by a probabilistic atlas. A probabilistic atlas is a structure that includes probability of each voxel to belong to each tissue type. Then, maximum likelihood approach is used to assign a label to each voxel for brain segmentation .

2.4. Atlas registration based on active contours

The third method is to integrate the statistical knowledge of intensity and position information of the atlas into a shape model and match the test data with this model, usually by active contours. An active contour model is proposed in [17] to perform lung segmentation for MRI scans. Gradient Vector Flow (GVF) is used to modify Partial Differential Equation (PDE) and attract shape contours to the actual shape model. The method also takes the advantage of prior information about the object location. In [19], an active contour scheme is developed for cardiac MRI segmentation. The main advantage of this method is the utilization of the region-based information as well as the edge information to decrease the sensitivity of the active contour method to the initial contours. In [20], a method based on simplex meshes is proposed for musculoskeletal segmentation and registration. A generic

model is introduced initially and the prior shape information such as smoothness and curvature is used during segmentation. The shape and deformation of the model are controlled by a deformable framework. This method is one of the first attempts in this field and need a manual initialization and user interaction makes this method less automatic. In [21], a shape model is constructed for masseter muscle by the help of several shape determinative slices. By using shape determinative slices authors try to address the problem of similar intensity values of neighbor tissues in some of MRI slices. These slices are specified and segmented manually. Then a hybrid method based on B-Spline and distance map is proposed to perform interpolation of the shape components. This study shows that the number of determinative slices highly effects the segmentation accuracy. The accuracy is 83% when 5 slices are used and it increases to 90% when 10 slices are used.

All these methods are highly dependent to initial shape model and initial contour locations. Prior knowledge is mostly introduced by manual segmentation.

2.5 MRF models

Fourth way is to incorporate the atlas as the initial labeling in a MRF (Markov Random Field) or a HMRF (Hidden Markov Random Field) model. MRF models are commonly used for unsupervised segmentation of medical data since smoothness constraint can easily be incorporated to the model by neighboring relations among the pixels to be segmented. The first studies of brain segmentation use the basic MRF-HMRF formulation where smoothness is defined based on the resemblance of the neighbors [22-23]. Then iterative methods like ICM (Iterated Conditional Model) are used to find the most probable labeling. In soft tissue segmentation, standard MRF modeling may not be applied directly since the parameters of the model need to be tuned for each new image. To improve standard MRF models, segmentation and registration are joined in [24]. This method aims to improve segmentation and registration accuracy by incorporating registered MRI sets in a combined MRF model and estimating the labels in a registration criterion. It is shown that by using this combination, the computational cost of registration is

reduced and there is a sizable improvement in segmentation of human brain and mouse heart. However this method needs the initial prior models to be set precisely.

In [25], distributed MRF segmentation is proposed to cope with spatially varying intensity distributions. Three different distribution classes are defined for MRI brain segmentation. The main problem in this approach is to find a partition that only includes these three classes. A new template for infant brain and the corresponding probabilistic atlas is constructed in [26]. The probability of each voxel for each class is determined by defining a HMRF model. Then a Maximum a Posteriori (MAP) is achieved by alternating among the classifications.

In [27], MRF distribution parameters are defined based on fuzzy MRF modeling and then the parameters of each class are estimated by using a nonlinear conjugate gradient method. The authors used the proposed method for detection of prostate cancer from MRI scans.

However the usual way of improving the MRF performance in segmentation is to use parametric model where the parameters are learned from the image usually by EM (Expectation Maximization) algorithm [25,27,28]. A HMRF model is developed in [28] to segment brain MR images where the EM algorithm is used to estimate the HMRF model parameters by solving Maximum Likelihood (ML) problem. Since there is no prior information used in this method, the algorithm is highly sensitive to noise and therefore is not robust. A commonly preferred method to incorporate the prior information to the MRF models is to register the atlas to the test image and to define the initial segment labels of the test image by the transformed atlases.

In [29], a probabilistic atlas is constructed by using manually segmented train images. Then this atlas is used in initialization and also in expectation step of the EM algorithm. In [30], each tissue type is appeared based on the transformed atlas to obtain the probability of each tissue type for each voxel. The initial class labels are assigned by choosing the maximum probability tissue type. Then the classification algorithm is used to locally maximize mutual information by changing the class of each voxel. The mutual information is defined based on Markov

probability density function (PDF). Initial class labels are used as the prior probability of the labels for brain segmentation.

Similarly, in [16], the brain atlas represents the prior probability of each voxel in the test set to belong to a particular structure. Then the Maximum likelihood function is defined by using Bayesian formulation so that the mutual information between the MRF model and the intensity distribution of the labeled atlas is maximized. In both studies, atlases are formed by manual segmentation.

A manually constructed probabilistic atlas is used in [13] to estimate the initial model parameters which are used as the priori information in the classification process. The segmentation algorithm incorporates spatial and temporal contextual information by using 4D Markov Random Fields. Finally, the expectation maximization (EM) algorithm is used to perform segmentation on cardiac MR images. In [31], atlas is used as a guide to perform population segmentation through population deformable registration. The atlas is registered to all of the test sets and the sets are deformed toward the atlas to achieve population segmentation. All sets are also registered and deformed to each other. The deformation is defined based on discrete MRF as pairwise potentials. Different from these studies, in [32], a latent atlas is used as the prior information where spatial priors are not in the form of probabilistic atlas. The atlas is initialized by a manual segmentation and then updated to be as the average of the segmentation result at each step of the level set segmentation.

Graph cuts are used to solve MRF problems in recent studies. This method can be used in medical image segmentation with some modifications so that the prior information can be included. In [33], a probabilistic atlas is first constructed by registering manually segmented training sets. The probabilistic atlas information is included in the energy function of the MRF formulation. The segmentation is achieved by an adaptive graph cut algorithm iteratively. A similar method is used in [34] but the tissue model is estimated directly from the test image and a mixture of Gaussians model is used to model different structures in the background. Both methods use manually segmented atlases to classify brain MRI to four classes.

In the literature, using the atlas as the prior probability of the labels is the most commonly chosen method to incorporate the prior information to the segmentation. However, this requires manually segmented atlases to be prepared. In this study, we propose another way for this cooperation where no manually labeled atlas is required.

2.6. Facial soft tissue segmentation

All methods mentioned above perform segmentation for soft tissues such as brain, lungs and cardiac. Very few studies considered Facial Soft Tissue (FST) segmentation for MR images.

In the literature, FST segmentation is mostly done for clinical purposes with manual or other simple segmentation methods where human interaction is required. In [35], manual segmentation of pelvic MRI scans is performed by clinical specialists and 3D models are reconstructed to identify pelvic disorders. Similar to that, in [36], extraocular muscles and corresponding cranial nerves are investigated with manual segmentation in patients with special forms of strabismus. Manual segmentation can also be combined with the help of segmentation tools as in [37-38] where Finite Element Model(FEM) of the face is constructed from facial MRI scans. In [39], a clinical study is presented which performs manual segmentation to investigate the differences in facial soft tissues between MuSK-MG patients and healthy people.

Anatomical visualization is another application of FST segmentation. In [40], one observer performs semi-automatic segmentation using the editor module of the 3D Slicer software [41] to segment lip muscles and reconstructs 3D models. Similarly in [42], the correlation between jaw muscle volume and vertical craniofacial dimensions are investigated. In this study Masseter and Medial Pterygoid (facial muscles) volumes and surfaces are segmented by semi-automatic segmentation tools.

Other than manual methods, there are some other automatic or semi-automatic methods studied for FST segmentation. Atlas based segmentation is a

method commonly used for brain segmentation and classification. There are several articles that use this method to segment other soft tissues. In [43], quadrates lumborum (QL) muscle(near pelvic) is segmented with an atlas based method. First an average atlas is constructed by affine registration of the sets and manual segmentation. Then atlas is registered to the test set by a non rigid registration technique and Kmeans classification algorithm is used to classify the image to different classes and the target tissue is segmented.

The main problem with classification algorithms in FST segmentation is the presence of several tissue types in one MRI slice. These tissue types may be different in the same slices from different individuals MRI. Therefore, the segmentation may result in wrong results or too many manual interactions are needed. Another atlas based method is used in [44] for prostate segmentation. The method is similar to [28] but an atlas selection strategy is used to select atlases that match the test data. The mutual information is selected as a metric to select the best matching atlases.

In [45], a novel method is proposed that uses an optimal path finding algorithm for facial nerve and chorda tympani (in ear) segmentation. The algorithm uses intensity and manually segmented atlas as feature values. The complete segmentation is performed using geometric deformation model.

Ng et al. [46-49] have tested several methods for FST segmentation based on prior knowledge. The main steps are similar in all of their studies. The process starts with manual segmentation of the training sets. Then registration from training sets to the test set is applied. The training images are transformed according to the difference between the shape of the head and the target tissue in each image and also tissue surface similarity. A tissue template is defined based on the transformed labeling. The muscle template is employed by the morphological operators to obtain an initial estimate of the muscle boundary. The muscle boundary then serves as the input contour to the gradient vector flow that snake iterates to the final segmentation. An improved method is proposed in [47] that shape determinative slices are used as a guide in 3D segmentation. A similar method is used in [46] with

a new method for determining the dominant slices of three human masticatory muscles (masseter, lateral andmedial pterygoids).

All these methods needs user interaction in several steps during the segmentation process. Also a thresholding method is used to exclude bone and fat that makes the method less automatic.

The complete and automatic segmentation of facial soft tissues still remains as an unsolved problem. In this work, we aim to investigate some of the methods which have been tested in segmentation of other soft tissues and try to modify them to be used in FST segmentation.

CHAPTER 3

THEORETICAL BACKGROUND

3.1. Introduction

In this chapter we provide the theoretical information about the methods that we used in this thesis. We start with the segmentation problem in medical images and explain the Markov Random Field theory and its application in image segmentation. Several statistical models are discussed for image target tissue modeling and the solutions for estimating the model parameters and performing labeling are reviewed. The role of prior information is also included in MRF modeling. At the end, several optimization methods for parameter estimation are explained.

Since we fused an MRF modeling with hidden atlas in our study, the concepts and procedures of atlas based methods are also discussed in this chapter. Since the first step of an atlas based method is the registration of the atlas and the test data, basic information about the registration is also mentioned at the end of this chapter after the explanation of the atlas based segmentation.

3.2. Labeling and Neighborhood Definition

An image segmentation problem is specified in terms of assigning a label to each member in the set of sites (pixels). Let S be a rectangular lattice for a 2D image of size n × n

$$S = \{(i, j) \mid 1 \le i, j \le n\} \ . \tag{3.1}$$

Each element of S corresponds to a pixel such that the location in the image space is specified by the indices i and j. In MRF models sites are normally treated as an unordered set but when a 2D image is modeled then i, j are ordered pixel locations

$$S = \{1, ..., m\}, \tag{3.2}$$

where m is the number of pixels in the image and is equal to n^2. Let L be a discrete set of M labels.

$$L = \{1, \cdots, M\} \tag{3.3}$$

Segmentation process is defined as assigning a unique value to each site in S in a way that whole domain of S is supported. So it's a mapping from S to L, that is

$$f : S \to L. \tag{3.4}$$

Then the set of labeling for all sites in S is shown as

$$F = \{F_1, ..., F_m\}. \tag{3.5}$$

As a result of segmentation, the image is partitioned into mutually exclusive regions where each region has a different label and all pixels in one region share the same label.

In this study we don't consider the whole image S, but we are interested to segmenting only a part of the image named as "the region of interest (ROI)" for which the definition and explanation are given in part 4.5.2 step 4. This ROI is segmented into two: target tissue and others (background). Thus, we define only two labels in L for the ROI. The background image is assigned by label 0 and the target tissue is assigned by 1. The total number of possible labelings for S becomes 2^m in this case.

Markov random field (MRF) is a probabilistic theory that represents the dependencies inside a physical phenomena [50]. It is used in visual labeling and probabilistic presentation of the labels in this study. Within a MRF model, sites are related to each other via a neighborhood system. A neighborhood system for S is defined as

$$N = \{N_i | \forall i \in S\}. \tag{3.6}$$

The neighborhood system can be defined in several ways. Some three dimensional (3D) neighboring systems are shown in figure 3.1 for a pixel i and N_i. In (a), 6 nearest neighbors in 3D space is shown. 8 nearest neighbors in one slice and the neighbors in upper and lower slices are selected as neighbors in (b). In (c) our proposed neighboring system is introduced where the neighbors are not only from the current 3D image but also from the images of other training sets. In this system, the corresponding voxels in the training sets are assumed as neighbors for the current voxel and affect the labeling of this voxel. Training set is a 2 dimensional image that is registered to the test set by an affine registration so both images share the same coordinates. The registration process is explained in part 3.6.3.

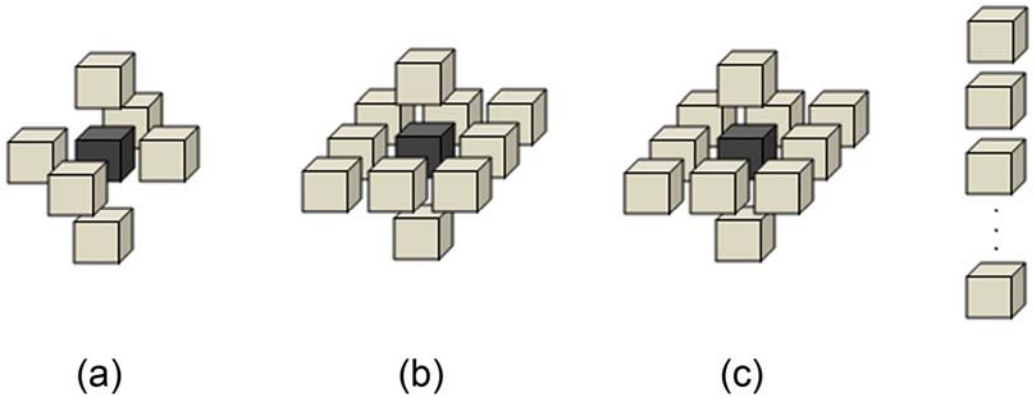

Figure 3.1 Neighboring systems with a) 6 neighbors, b) 10 neighbors, c) 19 neighbors

A clique is a group of voxels which are fully connected. A double clique c for S and N is defined as a subset of sites S which has 2 neighboring sites.

$$c_2 = \left\{ \{i, i'\} \middle| i' \in N_i, i \in S \right\} \tag{3.7}$$

Cliques have different cites but only single and pair-wise cliques are considered in this study.

3.3. Markov Random Field and Gibbs distribution

3.3.1. Markov Random Field

Let $F = \{F1,...,Fm\}$ be a family of random variables defined on the set S, each F_i takes a value f_i in L. We call the family F a random field. $F_i = f_i$ refers to the event where F_i takes the value f_i and the donation $(F_1 = f_1,...,F_m = f_m)$ is used to denote the joint event. For simplicity, a joint event is shown as $F = f$. The probability that random variable F_i takes the value f_i is abbreviated as $P(f_i)$, and the joint probability is denoted and abbreviated as $P(f)$. Random field F is said to be MRF on S with neighborhood system N if and only if:

$$1.\ P(f) > 0, \forall f \in F \tag{3.8}$$

$$2.\ P(f_i \middle| f_{S-\{i\}}) = P(f_i \middle| f_{N_i})$$

An MRF is said to be homogeneous if $P(f_i \middle| f_{N_i})$ is regardless of the relative position of site i in S.

3.3.2. Gibbs Random Field

A set of random variables F is said to be a Gibbs random field (GRF) with respect to N if and only if its configurations obey a Gibbs distribution. A Gibbs distribution takes the following form

$$P(f) = Z^{-1} \times e^{-\frac{1}{T}U(f)}, \tag{3.9}$$

where T is a constant named temperature, and $U(f)$ is the energy function. Z is the normalization term that is defined as

$$Z = \sum_{f \in F} e^{-\frac{1}{T}U(f)}. \tag{3.10}$$

The energy function is the sum of clique potentials $V_c(f)$ over all possible cliques.

$$U(f) = \sum_{c \in C} V_c(f) \tag{3.11}$$

When $V_c(f)$ is independent of the relative position of the clique c in S, the GRF is said to be homogeneous and when V_c is independent of the orientation of c, it is said to be isotropic.

For discrete labeling problems, if $f_c = (f_i, f_{i'}, f_{i''})$ be the local configuration on a triple-clique $c = \{i, i'i''\}$, then $V_c(f)$ can be specified by a finite number of parameters and f_c takes a finite number of states.

A Markov Random Field is characterized by its local property whereas a Gibbs Random Field is characterized by its global property. The Hammersley-Clifford theorem [51] gives necessary and sufficient conditions under which the equivalence of these two types of properties can be achieved. It states that F is an MRF on S with respect to N if and only if F is a GRF on S with respect to N. Then the energy function of the Gibbs distribution can be expressed as the sum of several terms. Each term is described by the cliques of a certain size.

$$U(f) = \sum_{\{i\} \in C_1} V_1(f_i) + \sum_{\{i,i'\} \in C_2} V_2(f_i, f_{i'}) + \sum_{\{i,i',i''\} \in C_3} V_3(f_i, f_{i'}, f_{i''}) + \ldots \tag{3.12}$$

And the conditional probability can be written as follows:

$$P(f_i \mid f_{N_i}) = \frac{e^{-[V_1(f_i)+\sum_{i' \in N_i} V_2(f_i, f_{i'})]}}{\sum_{f_{i \in L}} e^{-[V_1(f_i)+\sum_{i' \in N_i} V_2(f_i, f_{i'}]}} . \quad (3.13)$$

Different MRF models are introduced for modeling image properties like auto models, multi-level logistic model and hierarchical GRF Model. Auto models are simple and have low computational cost. An auto-model is used in this study for modeling image properties and general information about auto models are introduced next.

3.4. MRF Models

3.4.1. Auto-Models

Auto-models are encoded in the Gibbs energy as clique potentials of up to two sites. Then the energy function is defined as

$$U(f) = \sum_{i \in S} V_1(f_i) + \sum_{i \in S} \sum_{i' \in N_i} V_2(f_i, f_{i'}) . \quad (3.14)$$

This energy function involves up to pair-site cliques and called a second order energy. In the above formulation $\sum_{i \in S}$ is equal to $\sum_{\{i\} \in C_1}$ and $\sum_{i \in S} \sum_{i' \in N_i}$ is equal to $\sum_{\{i,i'\} \in C_2}$.

Let $G_i(.)$ be an arbitrary function and $\beta_{i,i'}$ be a constant reflecting the pair-site interaction between i and i'. Then if $V_1(f_i) = f_i G_i(f_i)$ and $V_2(f_i, f_{i'}) = \beta_{i,i'} f_i f_{i'}$, the energy function becomes

$$U(f) = \sum_{\{i\} \in C_1} f_i G_i(f_i) + \sum_{\{i,i'\} \in C_2} \beta_{i,i'} f_i f_{i'} . \quad (3.15)$$

This model is called auto-models. If f_i's take on values in the discrete label set $L = \{0.1\}$, the auto-model is said to be an auto-logistic model and the corresponding energy function becomes as follows

$$U(f) = \sum_{\{i\}\in C_1} \alpha_i f_i + \sum_{\{i,i'\}\in C_2} \beta_{i,i'} f_i f_{i'} . \tag{3.16}$$

When N is the nearest neighborhood system on a lattice, the auto-logistic model is reduced to the *Ising model*.

If the f_i's take on values in the label set $\{0,1,...,M-1\}$ and every f_i has a conditionally binomial distribution of M trails and success probability of q, the auto-model is said to be an auto-binomial model.

$$P(f_i \mid f_{N_i}) = \binom{M-1}{f_i} q^{f_i} (1-q)^{M-1-f_i}, \tag{3.17}$$

where

$$q = \frac{e^{a_i + \sum_{i'\in N_i} \beta_{i,i'} f_{i'}}}{1 + e^{a_i + \sum_{i'\in N_i} \beta_{i,i'} f_{i'}}} . \tag{3.18}$$

Then the corresponding energy function for auto-binomial model takes the following form

$$U(f) = -\sum_{\{i\}\in C_1} \ln\binom{M-1}{f_i} - \sum_{\{i\}\in C_1} a_i f_i - \sum_{\{i,i'\}\in C_2} \beta_{i,i'} f_i f_{i'} . \tag{3.19}$$

When $M = 1$, it reduces to auto-logistic model.

When the label set L is the real line and the joint distribution is multivariate normal, the auto-model is called auto-normal model or Gaussian MRF. In this case the p.d.f is defined as

$$P(f_i \mid f_{N_i}) = \frac{1}{\sqrt{2\pi\sigma^2}} e^{-\frac{1}{2\sigma^2}[f_i - \mu_i - \sum_{i'\in N_i} \beta_{i,i'}(f_{i'} - \mu_{i'})]^2} . \tag{3.20}$$

The mean and variance parameters for this normal distribution are

$$E(f_i \mid f_{N_i}) = \mu_i - \sum_{i'\in N_i} \beta_{i,i'}(f_{i'} - \mu_{i'}), \tag{3.21}$$

$$\mathrm{var}(f_i \mid f_{N_i}) = \sigma^2 . \tag{3.22}$$

The joint probability is a Gibbs distribution

$$P(f) = \frac{\sqrt{\det(B)}}{\sqrt{(2\pi\sigma^2)^m}} e^{\frac{(j-\mu)^T B(j-\mu)}{2\sigma^2}}, \tag{3.23}$$

where $B = [b_{i,i'}]$ is the $m \times m$ interaction matrix whose elements are unity and off-diagonal element at (i, i') is $-\beta_{i,i'}$, *i.e* $b_{i,i'} = \delta_{i,i'} - \beta_{i,i'}$ with $\beta_{i,i} = 0$. Then the single site and pair site clique potential functions become in the following form

$$V_1(f_i) = (f_i - \mu_i)^2 / 2\sigma^2 \tag{3.24}$$

and

$$V_2(f_i, f_{i'}) = \beta_{i,i'}(f_i - \mu_i)(f_{i'} - \mu_{i'}) / 2\sigma^2 \tag{3.25}$$

3.4.2 Observation Models

An observation $d = \{d_1, ..., d_m\}$ is a rectangular array of pixel values in low level vision problems. In this case, each pixel in the observation set d takes a value in set D. D is usually in 8 bit form that takes the following values $D = \{0,1,...,255\}$, i.e., gray level pixel values.

An observation is usually not equal to the exact reality. It is a transformed version of an MRF realization f. The transformation is due to random factors like noise. The conditional distribution or the likelihood of f can be determined considering these factors. We can define a general model for observation by use of a blurring factor B, a linear or nonlinear transformation φ and a sensor noise ε. The general observation model then has the form of

$$d = \varphi(B(f)) \circ \varepsilon \tag{3.26}$$

where $\circ$ is an operation of addition or multiplication. This model can be simplified to

$$d_i = \varphi(f_i) + \varepsilon_i \tag{3.27}$$

where there assumed to be no blurring, linear transformation and independent additive Gaussian noise. Then the likelihood of f or the probability distribution of d given f is

$$P(d \mid f) = \frac{1}{\prod_i^m \sqrt{2\pi\sigma_i^2}} e^{-U(d|f)}, \tag{3.28}$$

where the likelihood energy $U(d \mid f)$ is

$$U(d \mid f) = \sum_{i \in S} (\varphi(f_i) - d_i)^2 / [2\sigma_i^2] \tag{3.29}$$

This is a simplified version of Gibbs distribution where energy is due purely to single-site cliques in the zero-th order neighborhood system and the clique potentials are $[\varphi(f_i) - d_i]^2 / [2\sigma_i^2]$.

3.4.3. The Smoothness Prior

By introducing smoothness we assume that physical properties in a neighborhood of space present some coherence and generally do not change abruptly. Smoothness constraints are often expressed as the prior probability or equivalently an energy term $U(f)$ in MRF models. For discrete case, when the solution f is locally smooth on c, that means that all labels f_c on a clique c take the same value, they come over a negative clique potential (cost); otherwise, they incur a positive potential in the energy term $U(f)$.

3.4.4 MRF Prior for Piecewise Constant Surfaces

For piecewise constant surfaces modeling, Multi level logistic models can be used. For more than one-site cliques, the clique potential is defined as

$$V_c(f) = \begin{cases} 0 & \text{if all sites in } c \text{ have the same label} \\ \zeta_c & \text{otherwise} \end{cases} \tag{3.30}$$

Here, ζ_c is a negative constant dependent on c.

Clique potentials depend only on the label assigned to the site for single site cliques

$$V_c(f) = V_1(f_i) = \alpha_1 \qquad \text{if } f_i = l \in L_d \tag{3.31}$$

where α_1 is a value that controls the labeling l. The higher α_1 causes the percentage of sites that have l labeling, to decrease.

When V_c is nonzero only for the pair-site cliques, the clique potentials become as

$$V_c(f) = 0 \qquad \text{for \#c} > 2 \tag{3.32}$$

$$V_c(f) = V_2(f_i, f_{i'}) = \upsilon_{20}[1 - \delta(f_i - f_{i'})] \tag{3.33}$$

where $\delta(.)$ is the Kronecker delta function and υ_{20} is the parameter against non-equal labels on two-site cliques. The prior energy is defined as the sum of all clique potentials as follows

$$U(f) = \sum_{i \in S} \sum_{i' \in N_i} \upsilon_{20}[1 - \delta(f_i - f_{i'})]. \tag{3.34}$$

3.4.5 MRF Texture Model

MRF texture models can be defined by the use of joint probability $P(f)$. $P(f)$ is the probability of the texture pattern f to occur. Different MRF models are used for texture modeling. For example, in the MLL model, the clique potential functions are used to define the probability of the texture pattern f. If all the clique potentials other than pair-wise are non-zero, the clique potential equation is as below

$$V_2(f_i, f_{i'}) = \begin{cases} \beta_c & \textit{if sites on } \{i, i'\} = c \in C_2 \textit{ have the same label} \\ -\beta_c & \textit{otherwise} \end{cases} \tag{3.35}$$

where C_2 is a set of pair-size cliques and β_c is the parameter that specifies the MRF model. When all $\beta_c = \beta$, the MRF model is anisotropic and tends to generate texture like patterns. If β_c is different for different clique sets, it generates blob-like regions. By increasing the β_c, the selected region becomes larger and has more smooth boundaries. The clique potential function above is used to calculate the probability $P(f)$ using the corresponding Gibbs distribution.

For Gaussian model we assume that the observation d_i follows a Gaussian distribution with parameters $\theta_i = \{\mu_l, \sigma_l\}$. When the class label $f_i = l$, the probability of d_i becomes

$$P(d_i \mid f_i) = \frac{1}{\sqrt{2\pi\sigma_l^2}} e^{-(\frac{(d_i-\mu_l)^2}{2\sigma_l^2})} \tag{3.36}$$

3.5. Optimization

In computer vision process, there is a various amount of uncertainties like noise and other degradation factors. For this reason, an exact solution for vision problems is nearly impossible and most of them are formulated as optimization problems. Each optimization process in computer vision has three basic issues that should be considered: problem representation, objective function definition and optimization algorithms. The problem representation concerns how to represent image features and also how to represent the solution. For example in our case (image segmentation), locations of voxels represent the solution.

The objective function measures the quality of the solution in terms of some goodness or cost to a real number. In our MRF model, the energy function defined for this model is the objective function that needs to be optimized. The energy function has two important roles in optimization based vision problems: one is to measure of the global quality of the solution and the other is to guide the optimal solution searching. In this regard, proper formulation of the energy function is essential in finding the correct solution. The third issue is how to optimize the objective function to the best solution. In the following subsections we will discuss some solutions for optimization issues.

3.5.1. Iterated Conditional Modes

Iterated conditional modes (ICM) is a deterministic algorithm which maximizes local conditional probabilities sequentially. The algorithm updates each f_i^k into f_i^{k+1}, by maximizing the posterior probability $P(f_i \mid d, f_{S-\{i\}})$ with respect to f_i . The point of ICM is to maximize $P(f_i \mid d_i, f_{N_i}^k)$ beside $P(f \mid d)$. Maximizing $P(f_i \mid d, f_{S-\{i\}})$ is equivalent to minimizing the corresponding posterior potential as following

$$f_i^{k+1} \leftarrow \arg\min_{f_i} V(f_i \mid d_i, f_{N_i}^k) \tag{3.37}$$

where

$$V(f_i \mid d_i, f_{N_i}^k) = \sum_{i' \in N_i} V(f_i \mid f_{i'}^k) + V(d_i \mid f_i) \tag{3.38}$$

For discrete L, posterior potential is evaluated for each $f_i \in L$ and the label causing the minimum value is chosen as the f_i^{k+1}. In a cycle of ICM the above is applied to each i. This process continues iteratively until the convergence.

3.5.2 Bayes Estimation

Bayes theory states that when both the prior distribution and the likelihood function of a pattern are known, the best solution that can be estimated is the Bayes labeling. For Bayes estimation, the posterior probability can be computed from the prior distribution and the likelihood.

$$P(f \mid d) = \frac{P(d \mid f)P(f)}{P(d)} \tag{3.39}$$

where $P(d \mid f)$ is the conditional p.d.f of the observations d and $P(f)$ is the prior probability of labelings f . Also $P(d)$ is the density of d . Minimizing the Bayes risk is equal to maximizing the posterior probability so the minimal Bayes risk of estimate f^* is equivalent to

$$f^* = \arg\max_{f \in F} P(f \mid d). \tag{3.40}$$

Above function is known as the MAP estimate. When d is constant, $P(f \mid d)$ is proportional to the joint distribution.

$$P(f \mid d) \propto P(f, d) = P(d \mid f)P(f). \tag{3.41}$$

Then the MAP estimate can be found by

$$f^* = \arg\max_{f \in F} \{P(d \mid f)P(f)\}. \tag{3.42}$$

The MAP-MRF labeling for segmentation problem can be summarized in the following steps:

1. Define the appropriate MRF representation of the problem.
2. Define the neighborhood system, the set of cliques, clique potentials and the likelihood energy.
3. Find the posterior energy.
4. Find the MAP solution from the posterior energy

3.5.3. MRF Parameter Estimation

After selection of the functional form of the MRF model, if the parameters are known the optimized labeling can be estimated by the optimization methods explained in the previous section. But if the involved parameters are not known and should be specified, then optimization algorithms should be involved both to estimate the model parameters and the labeling.

The estimation problem is defined as estimating the parameters, θ, of a single MRF, F, from the observed data d which is due to a clean realization, f, of that MRF. When noise exists in the image, the unknown noise parameters should be estimated too and this increases the complexity. Also existence of multiple textures in the image increases the complexity as well because a separate MRF should be used for each texture model. Sometimes, the number of the underlying MRFs is unknown and should be determined which makes the problem even more complicated.

If the parameter estimation is done when data is already labeled, this is called as the supervised estimation. Otherwise it is unsupervised.

3.5.4. Supervised Estimation with Labeled Data

When data corresponds to a previously segmented image, i.e. the labels of the image pixels are known, the parameter estimation is done *supervised*. In this case, the set of parameters, θ, for each MRF model, F, are estimated using the data which is a clean realization, f, of that MRF. Maximum Likelihood (ML) method is a supervised method that is widely used in literature for medical image segmentation.

When realization f of an MRF model is known, the maximum likelihood (ML) tries to find the maximum value for conditional probability $P(f \mid \theta)$, which is the likelihood of θ, or its log likelihood $\ln P(f \mid \theta)$.

$$\theta^* = \arg\max_{\theta} P(f \mid \theta) \tag{3.43}$$

or

$$\theta^* = \arg\max_{\theta} \ln P(f \mid \theta) \tag{3.44}$$

For a homogeneous and isotropic auto-logistic MRF model with the 4-neighborhood system and the parameters $\theta = \{\alpha, \beta\}$, the global energy function and the local conditional probability can be defined as follows:

$$U(f \mid \theta) = \sum_{\{i\} \in C_1} \alpha f_i + \sum_{\{i,i'\} \in C_2} \beta_{i,i'} f_i f_{i'} \tag{3.45}$$

$$P(f_i \mid f_{N_i}) = \frac{e^{\alpha f_i + \sum_{i' \in N_i} \beta f_i f_{i'}}}{1 + e^{\alpha + \sum_{i' \in N_i} \beta f_{i'}}}. \tag{3.46}$$

The likelihood function is in the Gibbs form

$$P(f \mid \theta) = \frac{1}{Z(\theta)} \times e^{-U(f|\theta)} \tag{3.47}$$

with the partition function

$$Z(\theta) = \sum_{f \in F} e^{-U(f|\theta)} \tag{3.48}$$

Here $Z(\theta)$ is also a function of θ. To maximize $P(f \mid \theta)$ we need to compute $Z(\theta)$, but evaluation of $Z(\theta)$ is intractable because of the combinatorial number of elements in the configuration space F. Because of this difficulty, maximum likelihood cannot be solved directly but approximate solutions are used to solve this problem. Pseudo-likelihood is one of the frequently used approximate methods.

3.5.5. Pseudo-Likelihood

For approximation, the energy function can be written in the following form where each node i is treated as being independent of the others given its neighbors. This is a valid assumption for a MRF:

$$U(f) = \sum_{i \in S} U_i(f_i, f_{N_i}) \tag{3.49}$$

Here $U_i(f_i, f_{N_i})$ is based on the configuration of the cliques between i and N_i. For only single- and pair-site cliques, energy function and conditional probability can be written as

$$U_i(f_i, f_{N_i}) = V_1(f_i) + \sum_{i':\{i,i'\} \in S} V_2(f_i, f_{i'}) \tag{3.50}$$

and

$$P(f_i \mid f_{N_i}) = \frac{e^{-U_i(f_i, f_{N_i})}}{\sum_{f_i} e^{-U_i(f_i, f_{N_i})}} \tag{3.51}$$

$$P(f \mid \theta) = \frac{e^{-\sum_i U_i(f_i, f_{N_i})}}{\sum_{f_i \in L} e^{-\sum_i U_i(f_i, f_{N_i})}} \tag{3.52}$$

Then the pseudo-likelihood is defined as

$$PL(f) = \prod_{i \in S - \partial S} P(f_i \mid f_{N_i}) = \prod_{i \in S - \partial S} \frac{e^{-U_i(f_i, f_{N_i})}}{\sum_{f_i} e^{-U_i(f_i, f_{N_i})}} \tag{3.53}$$

where ∂S is the set of boundary points of S in the neighbor system N. By using the conditional probability (3.46) in the equation above, the pseudo-likelihood

approximation for a homogeneous and isotropic auto-logistic model can be achieved as follows:

$$PL(f) = \prod_i \frac{e^{af_i + \sum_{i' \in N_i} \beta f_i f_{i'}}}{1 + e^{a + \sum_{i' \in N_i} \beta f_{i'}}} \tag{3.54}$$

which is not related to the normalization term Z. In general, pseudo-likelihood is not the true likelihood function because of the dependency between f_i and f_{N_i} but it a solvable approximation.

As an example for maximum pseudo-likelihood (MPL) estimation, consider the homogeneous and isotropic auto-logistic model described before. The logarithm of (3.54) is

$$\ln PL(f \mid \theta) = \sum_{i \in S - \partial S} \left\{ \alpha f_i + \beta f_i \sum_{i' \in N_i} f_{i'} - \ln(1 + e^{\alpha + \beta \sum_{i' \in N_i} f_{i'}}) \right\} \tag{3.55}$$

Then, the MPL estimation $\{\alpha, \beta\}$ is obtained by solving

$$\frac{\partial \ln PL(f \mid \alpha, \beta)}{\partial \alpha} = 0 \tag{3.56}$$

$$\frac{\partial \ln PL(f \mid \alpha, \beta)}{\partial \beta} = 0 \tag{3.57}$$

3.5.6. Mean Field Approximations

Mean field approximation can be used to approximate the behavior of MRFs in equilibrium. In general, the mean of a random variable X is given by $\langle X \rangle = \sum_X Xp(X)$. So the mean field $\langle f \rangle$ can be defined by the mean values

$$\langle f_i \rangle = \sum_{f \in F} f_i P(F) = Z^{-1} \sum_f f_i e^{-\frac{1}{T} U(f)} \tag{3.58}$$

In this method, the following assumption is made to calculate $\langle f_i \rangle$: The actual influence of $f_{i'} (i' \neq i)$ is approximated by the influence of $\langle f_{i'} \rangle$. When the field is in equilibrium, this assumption is reasonable. The equation (3.50) can be approximated by the mean field local energy expressed as follows:

$$U_i(f_i \mid \langle f_{N_i} \rangle) = V_1(f_i) + \sum_{i':\{i,i'\}\in S} V_2(f_i, \langle f_{i'} \rangle) \tag{3.59}$$

and the conditional probability approximation takes the form of

$$P(f_i \mid \langle f_{N_i} \rangle) = Z_i'^{-1} e^{-\frac{1}{T} U_i(f_i \mid \langle f_{N_i} \rangle)} \tag{3.60}$$

where Z_i' is called the mean field local partition function and defined as

$$Z_i' = \sum_{f_i \in L} e^{-\frac{1}{T} U_i(f_i \mid \langle f_{N_i} \rangle)} \tag{3.61}$$

The mean field approximation of the joint probability can be shown as the product of the mean field local probabilities

$$P(f) \approx \prod_{i\in S} P(f_i \mid \langle f_{N_i} \rangle) = \prod_{i\in S} Z_i'^{-1} e^{-\frac{1}{T} U_i(f_i \mid \langle f_{N_i} \rangle)} \tag{3.62}$$

Similarly, the mean field partition function can be shown as the product of the mean field local partition functions

$$Z \approx Z' = \sum_{f} e^{-\frac{1}{T}\sum_{i\in S} U_i(f_i \mid \langle f_{N_i} \rangle)} = \prod_{i\in S} \sum_{f_i} e^{-\frac{1}{T} U_i(f_i \mid \langle f_{N_i} \rangle)} \tag{3.63}$$

Unlike the pseudo-likelihood, in the mean field approximation, the mean values and the mean field conditional probabilities are computed iteratively.

Another approximation method for MRF parameter estimation is to use a least squares (LS) fit procedure that is explained with details in [50, 52].

3.5.7. Unsupervised Estimation with Unlabeled Data

In image segmentation, our data is an observation from underlying MRFs, which is initially unlabelled. To find the MRF parameters, we should use the realization of only that MRF so the image should be segmented. However to segment the image, the parameters of that MRF model should be available. So the problem is to choose between segmentation and estimation.

One strategy to solve this problem is to perform segmentation using some other techniques like clustering and then to estimate the MRF parameters from the

resulting labeling. This method may not result in the optimum solution because the labeling is performed without using the correct parameter values.

An improved method is to perform labeling-estimation iteratively. The basic idea is to choose initial labeling by using some scheme and estimate the parameters based on this labeling. The estimated parameters are then used to find a hopefully better labeling, and so on. A simultaneous segmentation and estimation scheme is explained below.

Assume that $L \in \{1,...,M\}$ is the possible labels and f represents a segmentation or labeling with $f_i \in L$ indicating the label of pixel i. The data space S is partitioned into M different labels by the segmentation f. In our case, M is known and equal to 2. This means that the image includes only the target tissue and the background. In completely unsupervised methods, M is also unknown and should be estimated.

In terms of the MAP principles, the problem can be formulated as

$$(f^*, \theta_f^*, \theta_d^*) = \arg\max_{f,\theta_f,\theta_d} P(f, \theta_f, \theta_d \mid d) \quad , \tag{3.64}$$

where d is the observation model, θ_f is a set of MRF parameters and θ_d is a set of observation parameters. Assuming that θ_f and θ_d are both uniformly distributed, there is no prior knowledge about their distributions. When θ_f and θ_d are independent of each other, the above equation is reduced to

$$\begin{aligned}(f^*, \theta_f^*, \theta_d^*) &= \arg\max_{f,\theta_f,\theta_d} P(d \mid f, \theta_d) P(f \mid \theta_f) P(\theta_f) P(\theta_d) \\ &= \arg\max_{f,\theta_f,\theta_d} P(d \mid f, \theta_d) P(f \mid \theta_f)\end{aligned} \tag{3.65}$$

Maximization of the above problem is generally intractable. However this problem is solvable when θ_d can be expressed as a function $\theta_d(f, d)$.

Assume that the observation model is $d_i = \varphi(f_i) + \varepsilon_i$ where $\varphi(f_i)$ is the gray level for type $I = f_i$, for example the mean of pixels labeled as I, and ε_i is additive identical independent zero-mean Gaussian noise. The image space is assumed to be composed of piecewise constant valued regions that are governed by an MRF

model. Then the noise variance for type I regions can be estimated as a function of f and d

$$\theta_d^*(f,d) = (\sigma_I^2)^* = \frac{1}{\#S^{(I)}} \sum_{i \in S^{(I)}} (d_i - \varphi(f_i))^2 \tag{3.66}$$

Here $\#S^{(I)}$ is the total number of pixels in type I region. When θ_d is given as a function of f and d, the (3.65) is reduced to

$$(f^*, \theta_f^*) = \arg\max_{f,\theta_f} P(d \mid f, \theta_d^*(f,d))\, P(f \mid \theta_f) \tag{3.67}$$

The minimization is still a difficult problem. The solution can be found by dividing the problem into two sub-problems

$$f^* = \arg\max_f P(d \mid f, \theta_d^*(f,d)) P(f \mid \theta_f^*) \tag{3.68}$$

$$\theta_f^* = \arg\max_\theta P(d \mid f, \theta_d^*(f^*,d)) P(f^* \mid d, \theta_f) \tag{3.69}$$

The estimate (f^*, θ_f^*) thus can be found by iteratively alternating between the two equations. There are several methods for solving this problem such as simulated annealing (SA) [53], heuristic ICM and Pseudo-likelihood. The general technique for finding maximum likelihood estimate with incomplete data is expectation-maximization algorithm [54]. This method will be completely explained in the following subsection.

3.5.8. Expectation-maximization

The expectation-maximization (EM) estimate is obtained from the complete data by maximizing the likelihood function

$$\theta^* = \arg\max_\theta \ln P(d_{com} \mid \theta) \tag{3.70}$$

The complete data is assumed to consist of two parts, $d_{com} = \{d_{obs}, \hat{d}_{hid}\}$, where d_{obs} is the observed data and $\hat{d}_{hid}$ is the hidden data. EM procedure attempts to solve the following ML estimation problem with using only the observed data

$$\theta^* = \arg\max_\theta \ln P(d_{obs} \mid \theta) \tag{3.71}$$

This problem is more general than the classic ML. Starting from some initialization for $\hat{d}_{hid}$ and θ, EM algorithm iterates between the following two steps until convergence:

(1) Estimate the hidden data, using the current θ and use it to form the complete dataset d_{com}.

(2) Estimate the parameters θ, by using d_{com} and maximizing the complete-data log likelihood $\ln P(\hat{d}_{hid}, d_{obs} \mid \theta)$.

The log likelihood function above is a random function of the hidden variables f and we cannot work directly with this function. So EM algorithm tends to use the complete-data log likelihood $E[\ln P(\hat{d}_{hid}, d_{obs} \mid \theta)]$ which formalizes the procedure above. The hidden data for MRF model parameter estimation is the unobservable labeling f and the observed data is the given data d. At each iteration, the EM algorithm consists of the following two steps:

(1) The expectation step (E-step): The following conditional expectation of the log likelihood is computed

$$\begin{aligned} Q(\theta \mid \theta^{(t)}) &= E[\ln P(f, d \mid \theta) \mid d, \theta^{(t)}] \\ &= \sum_{f \in F} p(f \mid d, \theta^{(t)}) \ln p(f, d \mid \theta) \end{aligned} \tag{3.72}$$

(2) The maximization step (M-step): $Q(\theta \mid \theta^{(t)})$ is maximized to obtain the next estimate

$$\theta^{(t+1)} = \arg\max_{\theta} Q(\theta \mid \theta^{(t)}) \tag{3.73}$$

In the expectation step the conditional expectation of the hidden labels f, given the observed data d and the current estimate $\theta^{(t)}$, is computed. Then the labels are substituted with the new ones. In the maximization step, maximum likelihood estimation is performed assuming that the data is complete, i.e., as hidden data had been filled in by the expectations.

For the Gaussian MRF model case, the intensity distribution function, given the parameter set θ, is

$$P(d_i \mid \theta) = \frac{1}{\sqrt{2\pi\sigma_l^2}} e^{-\frac{(d-\mu_l)^2}{2\sigma_l^2} p(l \mid f_{N_i})} \tag{3.74}$$

Here, $p(l \mid f_{N_i})$ is the locally dependent probability of $f_i = l$ and the parameter set is $\theta = \{\mu_l, \sigma_l \mid l \in L\}$.

Then the Q-function becomes

$$Q = \sum_{i \in S} \sum_{l \in L} \left\{ P^{(t)}(l \mid d_i) W + C \right\} \tag{3.75}$$

where

$$W = \ln p^{(t)}(l \mid f_{N_i}) - \ln \sigma_l - \frac{(d_i - \mu_l)^2}{2\sigma_l^2} \tag{3.76}$$

and

$$C = -0.5 \ln(2\pi) \tag{3.77}$$

The model parameters can be obtained by applying EM algorithm

$$\mu_l^{(t+1)} = \frac{\sum_{i \in S} P^{(t)}(l \mid d_i) d_i}{\sum_{i \in S} P^{(t)}(l \mid d_i)} \tag{3.78}$$

$$\left(\sigma_l^{(t+1)}\right)^2 = \frac{\sum_{i \in S} P^{(t)}(l \mid d_i)(d_i - \mu_l)^2}{\sum_{i \in S} P^{(t)}(l \mid d_i)} \tag{3.79}$$

It is shown that the EM estimates converge to the ML estimates at least locally under some conditions .

3.6. Atlas based segmentation

Prior information is an important concept in medical image segmentation. Atlas is the most preferred framework to include prior information to a segmentation task. An atlas is usually referred to as a mapping $A: R^n \rightarrow L$ from n-dimensional spatial coordinates to labels from a set of classes L. To segment a new image S, using an atlas A, a transform between them should be computed. To find the accurate transformation, two images should be registered to each other. The

registration from the atlas image to the target image should be non-rigid not only to change the image linearly, but also to change the shape of the objects in the atlas in a nonlinear way so that they can fit well to the corresponding objects in the target image. Important concepts in an atlas based segmentation are listed as follows and each is detailed in the following text.

- Atlas construction
- Atlas selection
- Image registration

3.6.1. Atlas construction

An atlas is usually generated by manual segmentation of training images. The atlas can be constructed from a single image or average of many images. Thus, construction of atlases is very time consuming and prone to error. For average atlas construction, all of the images should be registered to a reference image so that the corresponding objects in the image will share the same locations. This is done by an affine registration that is explained in the next chapter. For atlas construction the registration applies linear transformation to the images so it wouldn't affect the shape of the objects in the image.

3.6.2. Atlas selection

Different atlas selection methods are proposed and evaluated in the literature. Four important atlas selection strategies are shown in the figure 3.2.

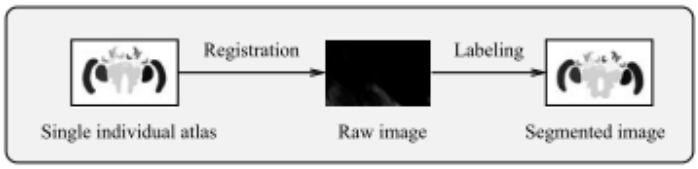

IND: Segmentation using a single individual atlas.

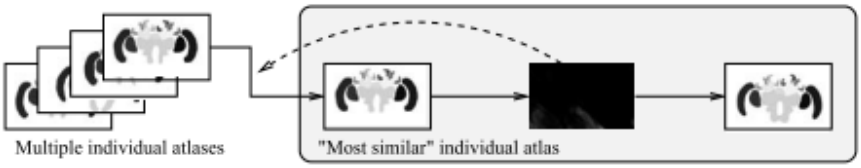

SIM: Segmentation using the "most similar" individual atlas.

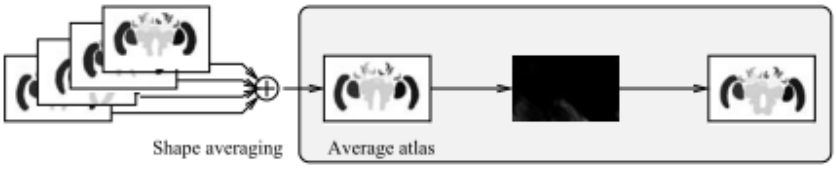

AVG: Segmentation using an average shape atlas.

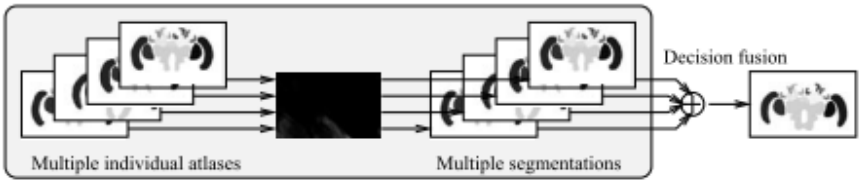

MUL: Independent segmentation using multiple individual atlases with decision fusion.

Figure 3.2 Atlas based segmentation strategies.

Segmentation with a fixed, single individual atlas is the most straight forward strategy for selection of an atlas. In this method, a single atlas is selected mostly randomly to perform segmentation. Usually there is a single atlas and thus atlas construction is simple and fast but it may result in a wrong segmentation if the objects in the atlas and the test images are very different from each other.

Another method is to select the most similar atlas to the test image. But the problem with this approach is that the correct segmentation for an un-segmented image is unknown. So the best atlas is usually selected by some similarity measures that may result in wrong answers.

Segmentation with an average shape atlas is performed by averaging several manually segmented atlases. This method considers different images with different shapes so that it decreases the risk an individual being an outlier in the population. But high amount of manual segmentation and registration increases the time and also the computational cost.

Multi atlas segmentation is done by performing segmentation for the test image with different atlases and then generating the resultant segmentation by combining all individual results. The simplest way to combine the individual segmentations is averaging. However, the success of the method depends on the performance of the fusion strategy, which could be different than only averaging.

3.6.3. Image registration

In addition to a spatial map of labels, the actual atlas also allows us to access to the corresponding realization of the image modality. So the registration is performed between two real images.

Image registration is to overlay two or more images with a linear or non-linear geometrical alignment. In medical image registration, input images can be images with different modalities from the same person. Such registration is done to obtain more complete information about the patient. Or they can be images from different individuals but with the same modality. Such registration is usually done to obtain average atlases from the training sets, which are then used as the prior knowledge in test image analysis. In this study, we consider images from different individuals but having the same imaging modality, i.e., imaging sensors and viewpoint of imaging.

The registration can be grouped into two general categories: rigid and non-rigid registration. Rigid registration is performed by a rigid transform with 6 degrees

of freedom (3 for rotation and 3 for translation). Affine registration is an improved form of rigid registration with 9 degrees of freedom that incorporates shearing into registration process. In rigid registration, the distance between the points remains constant. However, in non-rigid registration, the local deformation between the images is allowed involving a much larger number of degrees of freedom. A simple visualization of rigid and non-rigid registration is shown in Figure 3.3.

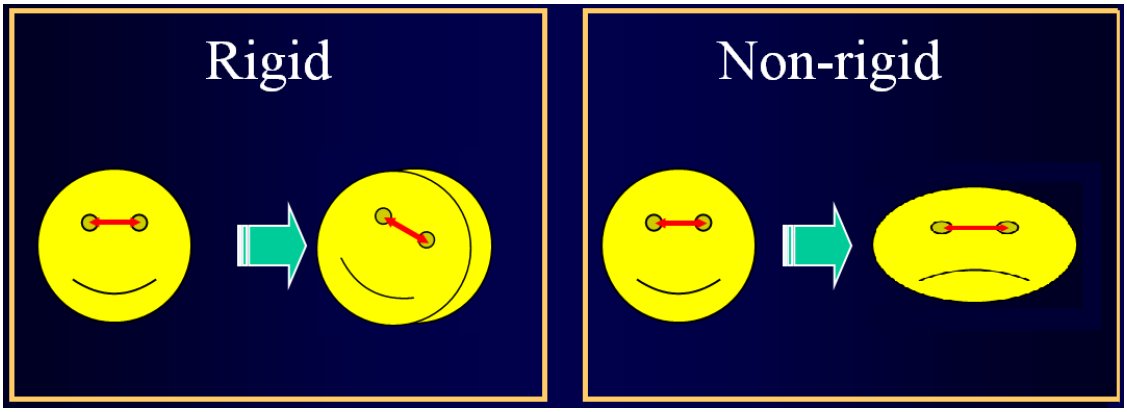

Figure 3.3 Rigid and non-rigid registration

Registration algorithms can be categorized in three groups:

- **Landmark based registration**: In this method, a group of landmark points are selected in both images by the user and mapping is computed between these corresponding points.
- **Feature based registration**: Some features, such as edges, corners or regions, are detected from both images mostly automatically and matching between these points are estimated. The mapping is computed between the corresponding points.
- **Intensity based registration**: Registration is performed by minimizing the intensity differences over the entire images.

Although landmark based registration may result in a more accurate transform, a large amount of human interaction is needed and the registration performance is directly related to the number of landmarks. For feature-based registration, some image features like edges and surfaces should be computed and matching between these should be estimated before the registration. When these are done automatically, performance is not very high. Manually segmented structures may be used as features for accuracy improvement but this decreases the automaticity of the method. Intensity based registration involves calculating the registration transformation by optimizing some measures computed directly from the voxel values. Choosing the proper similarity measure depends on the image modality. The most successful similarity measure for medical images is mutual information [55].

The mutual information of two discrete random variable X, Y is defined as follows:

$$I(X,Y) = \sum_{y \in Y} \sum_{x \in X} P(x,y) \log \left[\frac{P(x,y)}{P_1(x) P_2(x)} \right] \tag{3.80}$$

The registration is performed in a way that maximizes the mutual information between two images. Several optimization strategies have been proposed for mutual information maximization [56]. Some important multi resolution gradient- and non-gradient-based methods are Powell, simplex, steepest-descent, conjugate-gradient, quasi-Newton and Levenberg–Marquardt methods.

One of the efficient and robust intensity based registration techniques is demons registration [57]. In demons registration, the optical flow equation is used to find small deformations in image sequences. Let p be a point in reference image F, f be the intensity and m be the intensity in the moving image M. Then $u = (u_x, u_y)$ is defined as the estimated displacement required for point p to match the corresponding point M.

$$u = \frac{(m - f)\nabla f}{|\nabla f|^2 + (m - f)^2} \tag{3.81}$$

Where ∇f is the gradient of the reference image. Displacement u is based on local approximation so to register two images, so it should be solved iteratively. Mutual information can be used as similarity measure to optimize the registration.

CHAPTER 4

MATERIALS AND METHODS

4.1. Intro

In this chapter, the materials and methods that we used in this study are discussed. Our aim in this thesis is to investigate the role of prior information in medical image segmentation. For this purpose, we apply several present segmentation methods for two dimensional (2D) segmentation of target facial soft tissues. These methods are chosen because they are the representatives in the previous literature, which use prior information in some way or the other. A comparison between these methods will clarify different aspects of prior knowledge based segmentation methods. These methods are:

Method a. Atlas based segmentation,

Method b. MRF based segmentation with initials from region growing algorithm,

Method c. MRF based segmentation with initials from region growing algorithm using prior information,

Method d. MRF based segmentation using labeled atlas.

Then our newly proposed segmentation method, MRF based segmentation using unlabeled prior information (Method e), will be introduced and applied to the same image sets for 2D segmentation.

At the end, we propose a new framework that performs 2D segmentation for all of the slices of the data sets for the target tissue. As a result of this process a segmented three dimensional (3D) shape of target tissues are constructed with our proposed method.The methods are implemented using Matlab 7.10.0 on a computer with Intel Xeon 3.2 GHz (2 processors) CPU and 8 GB of RAM.

4.2. Target tissues

Four different facial soft tissues (FST) are selected as target tissues in this study: right Masseter (RM), left Masseter (LM), right temporalis (RT) and left Temporalis (LT).

Masseter is a strong and large muscle, responsible for jaw motion. An axial view of both right and left masseter muscles in an MR image is shown in figure 4.1. The muscle borders are specified in green. Temporalis is also a large facial muscle that assists in elevation of the mandible. Borders of Temporalis muscle is shown in Figure 4.2 in green.

We performed 2D segmentation for finding right masseter tissue with our method and other previous methods mentioned before and compared our results with them. We also performed 3D segmentation for 10 different MRI sets belonging to different individuals to find the four target tissues mentioned above.

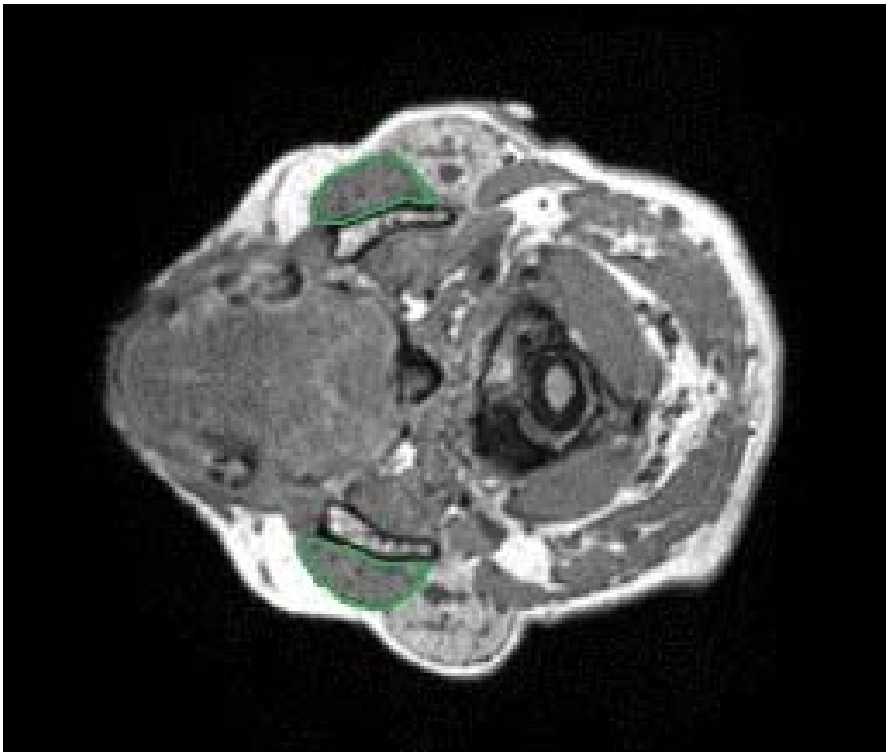

Figure 4.1 The target masseter tissues are shown by green.

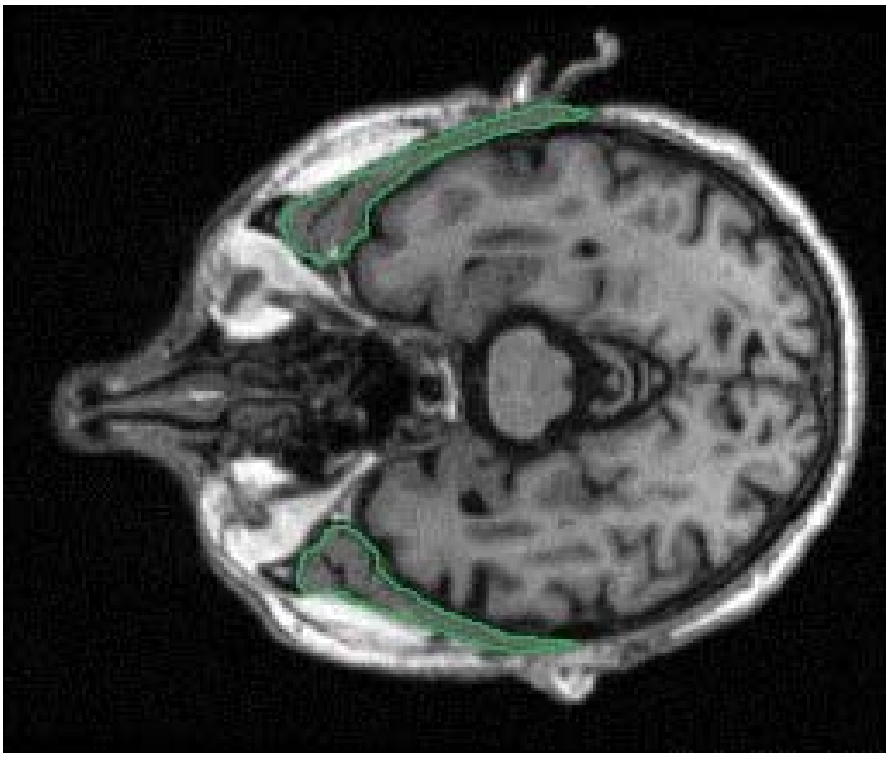

Figure 4.2 The target temporalis tissues are shown by green.

4.3. Train and test data

All the images used in this work were whole head and neck 3D MRI sets which are obtained from the Alzheimer's Disease Neuroimaging Initiative (ADNI) [58]. All image sets were axial T1 weighted sets with 1.2 mm slice thickness. Each set contain 256 slices with 256 x 217 pixels resolution. Ten different sets are selected as experimental data. In each experiment, leave-one-out technique is used, that is, each set is selected as the test set and the remaining sets are used as the training set. This process is repeated for all sets. Total of four FSTs, i.e., left masseter, right masseter, left temporalis and right temporalis, were selected as target tissues to be segmented.

4.4. Bias field correction

Magnetic resonance images are usually degraded by intensity in-homogeneity which is primarily because of the sensitivity profile of the radio frequency coil [59]. This phenomena is named intensity bias field and is characterized by multiplicative smooth spatial variations that modulate the intensity of the true image data. This causes a problem in image analysis techniques like segmentation and registration. To solve this problem, histogram equalization method is used as explained in [60]. In this method, histogram of all images are calculated and the average histogram is equalized. Then the intensity values of pixels in each slice are remapped to the new intensity value.

4.5. 2D segmentation

In this part we apply segmentation methods mentioned in section 4.1 for segmentation of masseter muscle in one single MRI slice. Each method is explained in this section where the result of a selected slice is also shown. Ten different MRI sets are selected as the experimental data. All these sets are registered in 3D by an

affine registration method so the slices will correspond to each other. A single slice is selected from each set to perform 2D segmentation, i.e., 10 slices in total. We use leave-one-out technique where one of the slices is selected each time as the test data to be segmented and the other 9 slices are selected as the training sets that are used as the prior information. A sample of input image for our system is shown in figure 4.3. The visual results of each segmentation process will be shown for this particular image.

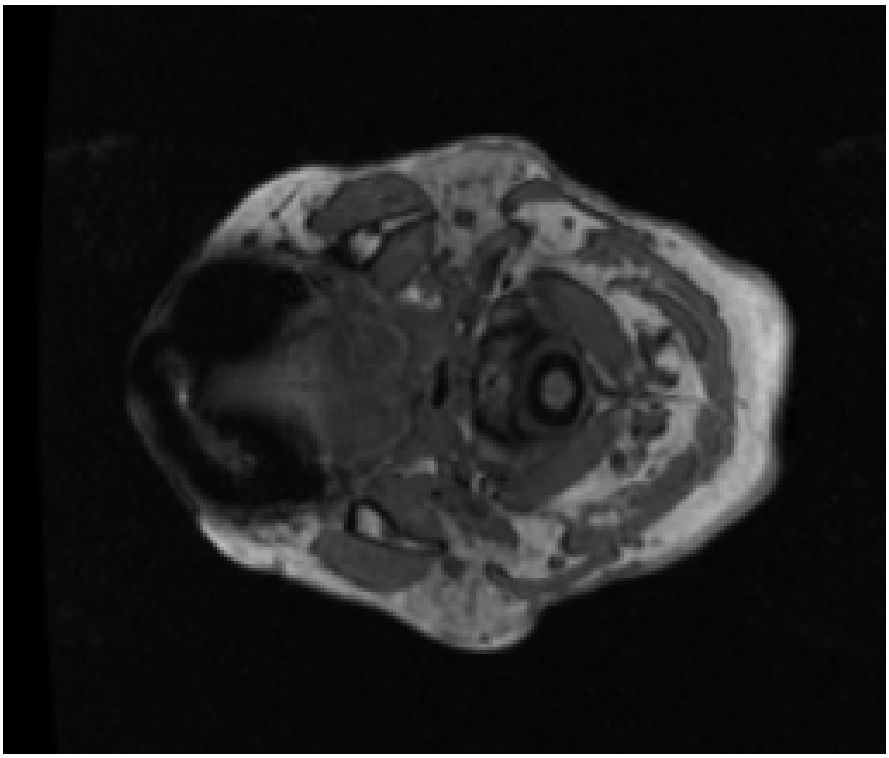

Figure 4.3 Sample MRI slice that is used for visualization in this thesis.

4.5.1. Method a: Atlas based segmentation

Atlas based segmentation is one of the popular methods in medical image analysis, especially in brain soft tissue segmentation [43, 61-62]. The basic concepts of this method are explained in part 3.6. An overview of this method is shown in figure 4.4.

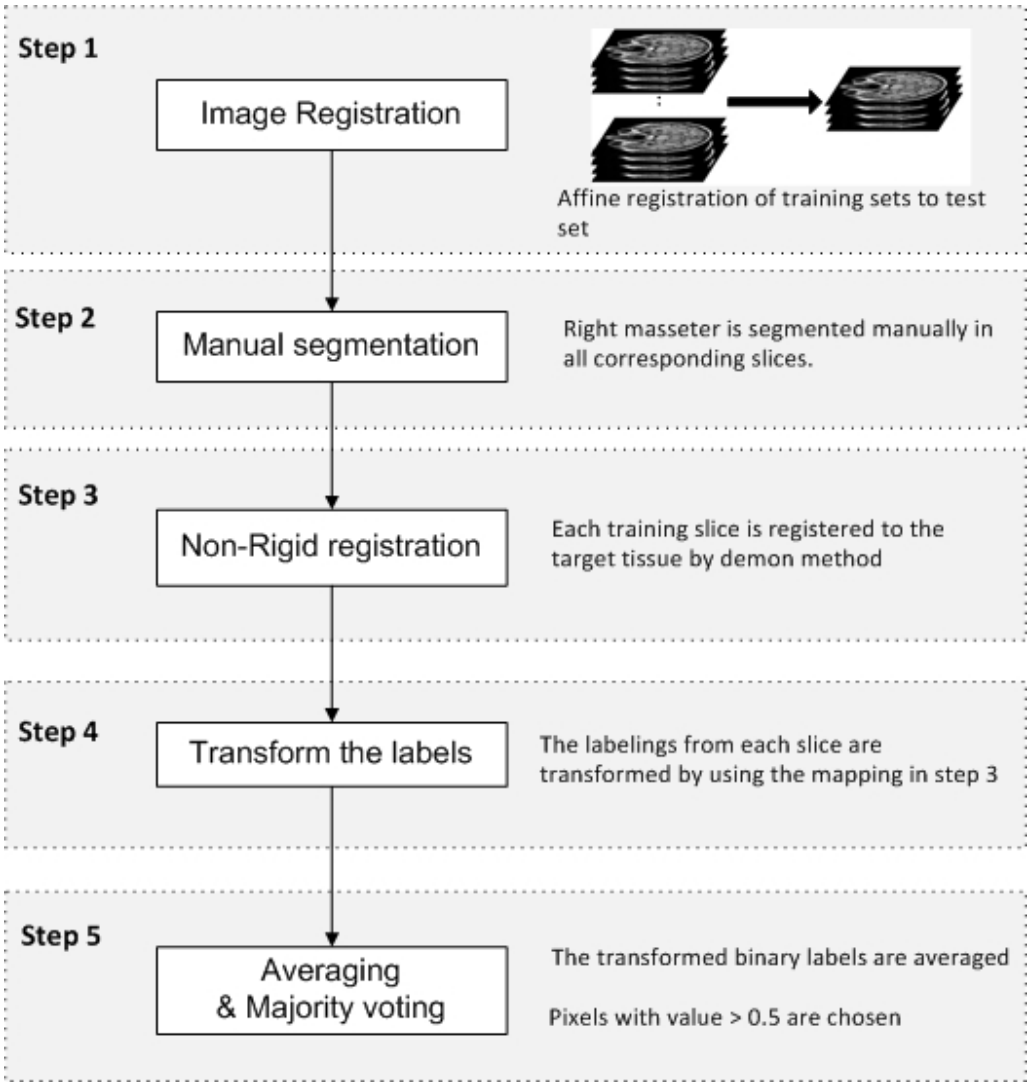

Figure 4.4 Overview of method a.

The system is composed of the following steps:

Step 1: Image registration: All MRI sets are registered to a randomly selected set with an affine registration. Normalized mutual information is used as similarity measure in the registration process. The registration is performed by using Amira software [63].

Step 2: Manual segmentation: The masseter muscle is then segmented in selected slices manually. The manual segmentation is performed by a professional user.

Step 3: Non-Rigid registration: To find a mapping from each image in the training set to the test set, a registration from the train set to the test set should be applied. The applied registration method is the demon registration that is explained in section 3.6.3. By applying the non-rigid registration, target tissue in the training set tends to change shape toward the shape of the tissue in the test set. This process is done for all of the 9 training data.

Step 4: Transform the labels: In step 3, we obtained a transformation from each train set to the target set. In this step, the obtained transforms are applied to the corresponding labeling images. So the label image will also change the shape to fit the test set.

Step 5: Averaging and majority voting: To obtain the overall segmentation of the test set, an average image is made from the labels produced in step 4. The average image is shown in figure 4.5. The bright locations that are repeated in more images are brighter in this image. By performing majority voting procedure on the average image, we select the pixels that are repeated more than 4 times out of total 9 images.

Manual segmentation of each slice is needed for this method that is so time consuming and increases the overall time of segmentation. Other than that the average time for non-rigid registration from a training set to the test set is 189 seconds. Without considering manual segmentation, the algorithm takes baout 1713 seconds to perform segmentation for one slice. The segmentation result for the input image is shown in figure 4.6. The border of the segmented region is shown in blue.

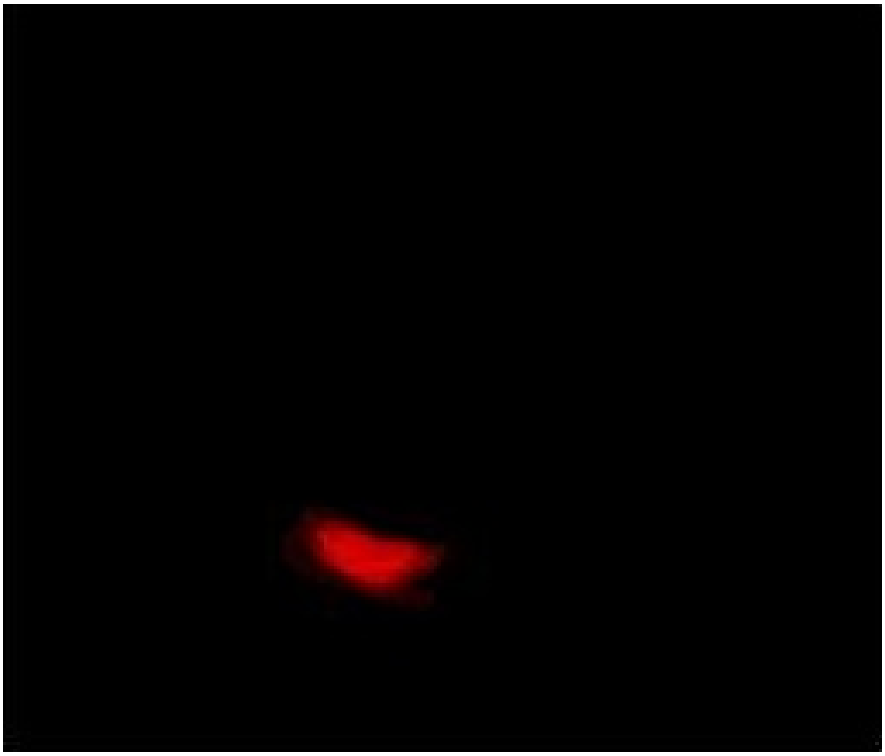

Figure 4.5 Average image from manually labeled training images

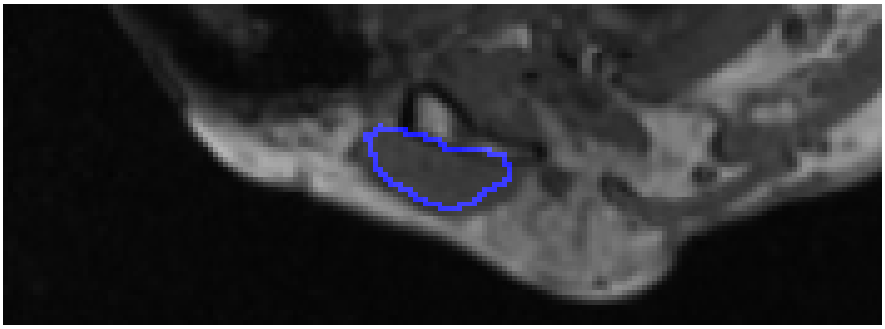

Figure 4.6 Result for the sample image by using method a.

4.5.2. Method b: MRF based segmentation with initials from region growing algorithm

Markov random field framework is a favored technique to encode spatial information in an image through contextual constraints of neighboring pixels. We seek to find the maximum a posteriori estimate of the segmentation by using expectation maximization (EM) algorithm. The method is explained in section 3.5.8. A problem in MRF based segmentation of facial soft tissues is that, in MRF modeling, tissues with the same intensity distribution are modeled in the same group. This method is mostly used in classification of brain soft tissues where whole image can be classified into different classes. However in FST segmentation we want to label a single tissue without adding the other tissues with similar distribution. To solve this problem a rectangular region of interest (ROI) is selected around the target tissue and the segmentation is performed only on this ROI. The method by which the ROI is selected will be explained in part 4.5.2 step 4.

In this section, we try to perform MRF based segmentation without using any prior information. This will help us to understand the basic MRF segmentation, which is considered as a baseline, and the effect of prior information, when it will be introduced later, in the MRF segmentation process. The segmentation process is like the method used in [28] that performs segmentation for brain MR images. The performance with this basic MRF approach is poor, because the convergence of the EM algorithm strongly depends on the initial labeling and parameters. Thus, different from [28], we use a region growing algorithm to find the initial labeling and compute the initial parameters from it. In this case, we mark a single pixel on the target tissue and we apply ordinary region growing so that an initial segment is obtained starting from this initial point. This segmentation is used as the initial labeling and then MRF is optimized to reach the final segmentation of the ROI. An overview of the method is shown in figure 4.7.

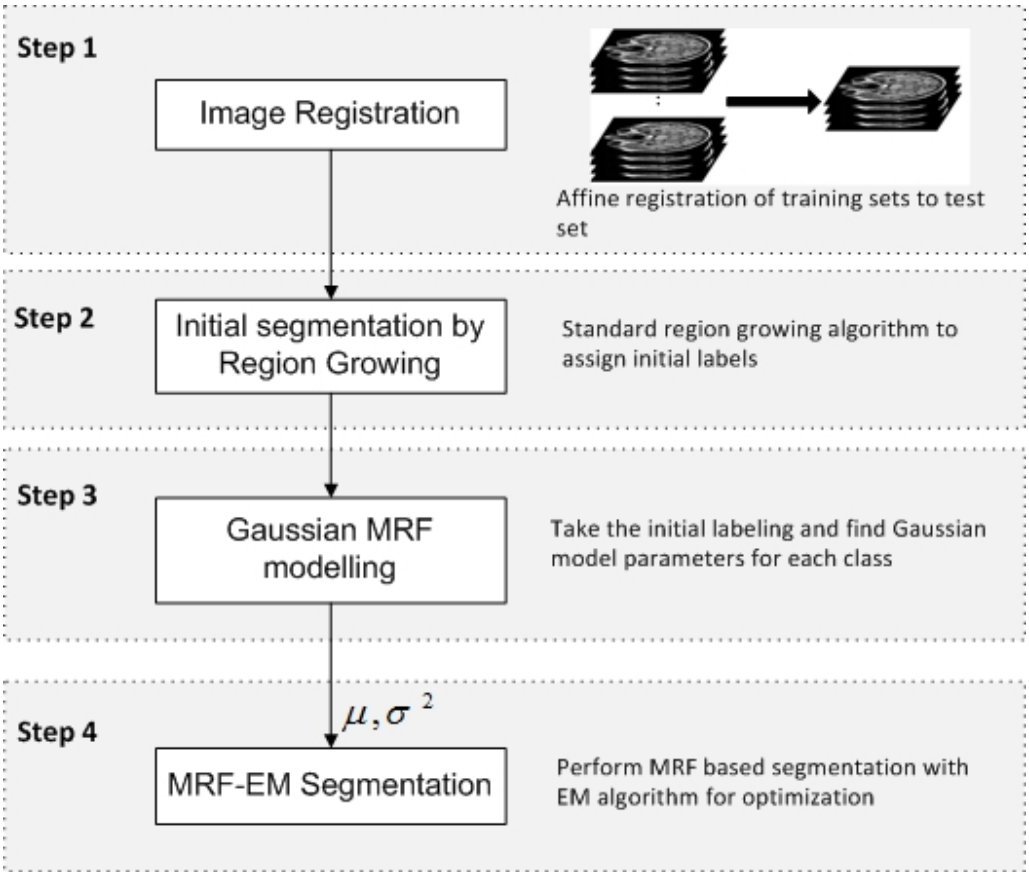

Figure 4.7 Overview of method b.

Step 1: Image registration: The same registration method as used in part 4.5.1 step 1 is also used here.

Step 2: Initial segmentation by region growing: Region Growing (RG) is one of the basic methods in image segmentation. In this method, algorithm starts from a starting point, called the seed point, that is selected by the user. Then the neighbors of the selected pixel are checked to obey a criteria, i.e., to have an intensity value similar to the selected point's value in this study. This process continues for the newly selected pixels and the difference between neighbor pixel intensity and the mean intensity of the selected pixels is computed and checked to be under a certain threshold. The process is repeated until there is no neighbor pixel left that obeys the criteria.

The threshold value is selected only once by the user but kept constant for the segmentation of all other slices. This constant value can be used for the segmentation of all slices because of the histogram equalization process that is applied to all of the slices prior to segmentation.

To summarize, RG is a simple semi-automatic method that uses an initial seed point and a threshold to segment a region in a 2D image by using only intensity information. The result of this step is a binary image that includes target tissue pixels (labeled as 1) and background pixels (labeled 0). The output of this step is shown in Figure 4.8.

Step 3: Observation model as a Gaussian: In this step, we aim to model two different classes of pixels for the binary image of step 3. We fit the target class and background class into separate Gaussian distributions and compute their parameters, i.e., mean and variance, μ, σ^2. Together with the labeled image, this information is passed to the next step where the segmentation process use them as the initial estimation.

Step 4: MRF-EM segmentation: As mentioned before, the MRF-EM algorithm performs classification for the ROI. The ROI is selected as a rectangle 5 times bigger than the bounding box of the initially labeled image. This size is big enough to cover masseter tissue in all cases and small enough to avoid other similar tissues. Although there are some other neighboring tissues with the same intensity distribution, this is inevitable. The centroid of the ROI is selected as the centroid of the segmented part in the labeled image.

The ROI is modeled as a Gaussian MRF as explained in part 3.4.1 with $L = \{0,1\}$. EM algorithm is used in this step to maximize the likelihood function defined in equation 3.29. The algorithm computes the posterior probability of the pixels for each class in the E-step by using initial parameters and then estimates the new Gaussian parameters using that probability in the M-step. The new parameters are used again in the E-step and this process continues until the maximum likelihood change between successive iterations becomes very small (i.e., less than 0.001 in this study).

The energy function is defined as equation 3.35 and the 8 nearest neighbors in the slice are selected as the neighboring system. This process converges to a result that contains two classes of pixels and it is an optimized version of the initial labeling. This method is also applied to 10 MR images from the experimental dataset. The initial labeling process takes 1.3 seconds by using region growing algorithm. The MRF-EM segmentation process takes 6 seconds that makes the overall computation time of this method to be 7.3 seconds for each slice. The final result for one image is shown in figure 4.9 where boundary of the target tissue is shown in blue.

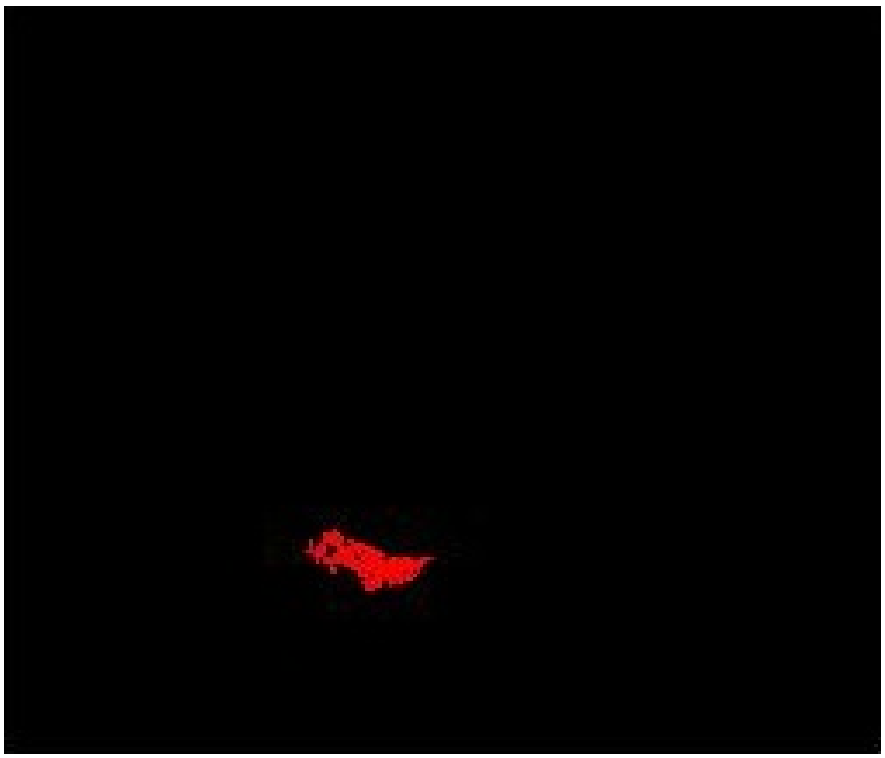

Figure 4.8 Initial segmentation result by region growing algorithm.

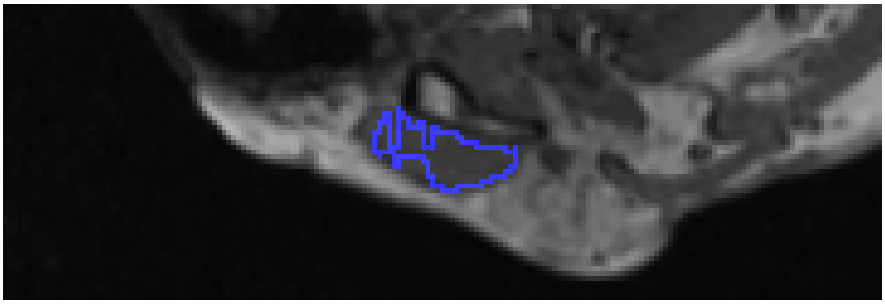

Figure 4.9 Result for the sample image by using method b.

4.5.3. Method c: MRF based segmentation with initials from region growing algorithm using prior information

To investigate the effect of the initial estimate in MRF based segmentation and also to be fair in comparison between MRF-EM method and our proposed method, we perform MRF based segmentation with initials obtained from a new modified region growing algorithm. This method is similar to the previous method explained in section 4.5.2 except that the region growing algorithm in this section is a modified version of the basic form described in the previous section.

An overview of the algorithm is shown in figure 4.10. The method consists of the following steps:

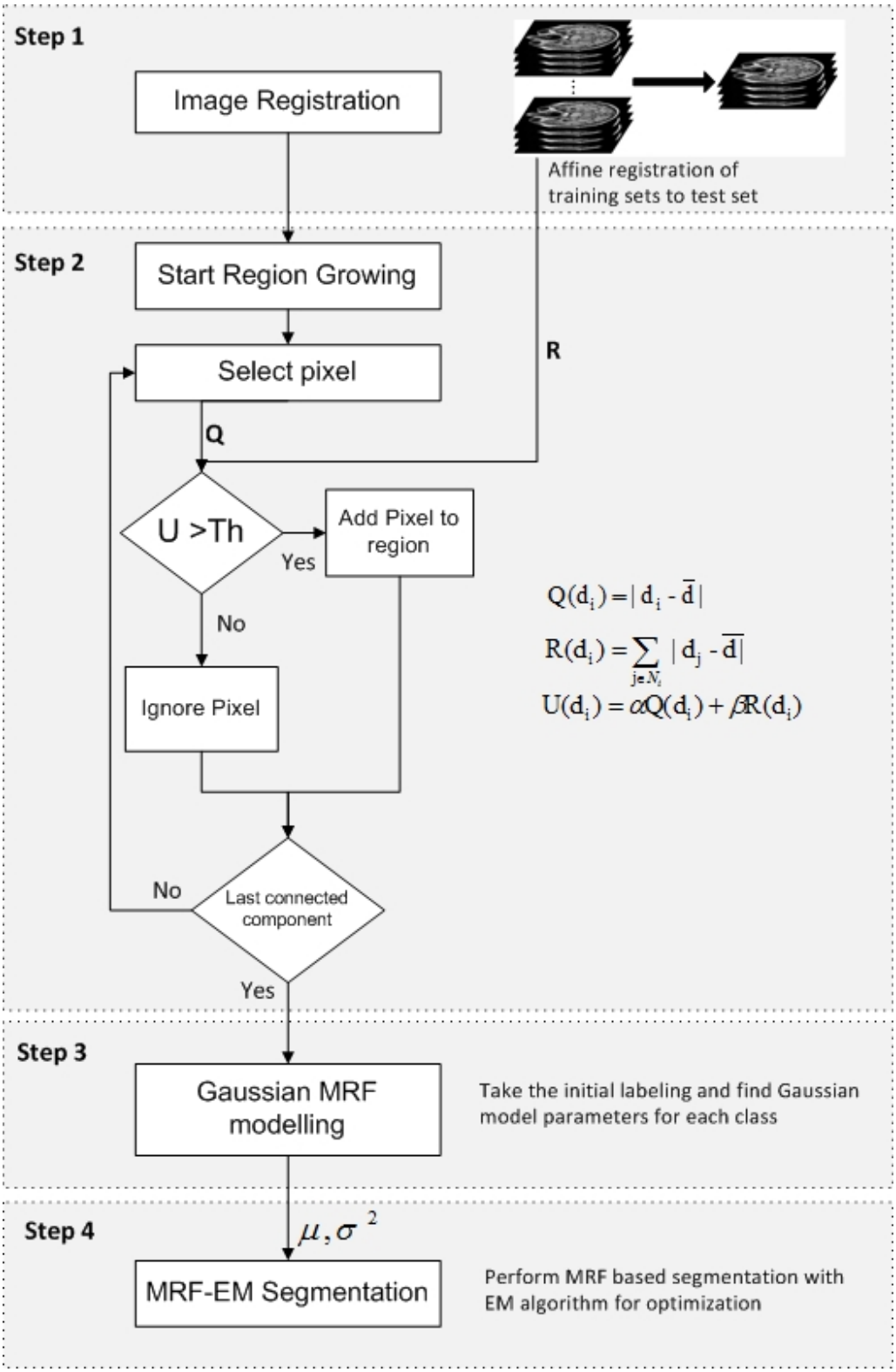

Figure 4.10 Overview of method c.

Step 1: Image registration: The registration method is the same as the one applied earlier.

Step 2: Initial segmentation by region growing: The region growing algorithm in this step is a modified version of the basic region growing method to take the advantage of prior information. In this case, region growing is done not only by considering the neighboring pixels on the same slice but by considering the corresponding pixels in the other data sets, i.e., training sets, although they are not segmented a priori. Since the training sets are registered, they share the same coordinates and hopefully have the same locations for target structures.

We assume that pixels are connected to each other through the neighboring system shown in figure 3.1(c). This means that the current pixel is connected to the corresponding pixels in the upper and lower slices and 9 other training images as well as 8 nearest neighbors in the same slice. These 19 neighbor pixels effect the classification of the current pixel. It can be said that when a pixel is being checked in the RG algorithm, a corresponding pixel in the training set with intensity value similar to the tissue mean should increase the probability of the current pixel to be included to already segmented region. The new criterion $U(d_i)$ is defined in a way that preserves the circumstances above:

$$Q(d_i) = |\, d_i - \bar{d}\,| \tag{4.1}$$

$$R(d_i) = \sum_{j \in N_i} |\, d_j - \overline{d}\,| \tag{4.2}$$

$$U(d_i) = \alpha Q(d_i) + \beta R(d_i) \tag{4.3}$$

Here d_i is the current pixel and d_j is the neighbor pixel from the neighboring set N_i. $\bar{d}$ is the intensity mean of the pixels of the already segmented region in the current step. The term $Q(d_i)$ represents the criteria that was used in method b region growing algorithm and involves the comparison of only the intensity value of the current pixel. The term $R(d_i)$ represents the influence of the neighboring pixels. Two parameters α and β control the effect of each term Q and R. α and β are set manually and kept constant throughout the experiments. The algorithm checks

U for each pixel to be lower than a preset threshold and proceeds as in the original RG algorithm. The resultant labeling image is shown in figure 4.11.

Step 3: Observation modeling by Gaussian: This part is similar to step 3 of section 4.5.2.

Step 4: MRF-EM segmentation: This step is similar to step 4 of section 4.5.2. The energy function is defined only in the current slice just like the previous case and no prior information is used in the segmentation.

Although prior information is not used in the segmentation process of this method, it is included in initialization of the model estimation. So this method can't be called a prior free method. The initial labeling process takes 2.2 seconds by using the new region growing algorithm. The MRF-EM segmentation process takes 6 seconds that makes the overall computation time of this method to be 8.2 seconds for each slice. The segmentation result is shown in figure 4.12. The boundary of the segmented area is shown in blue in the figure.

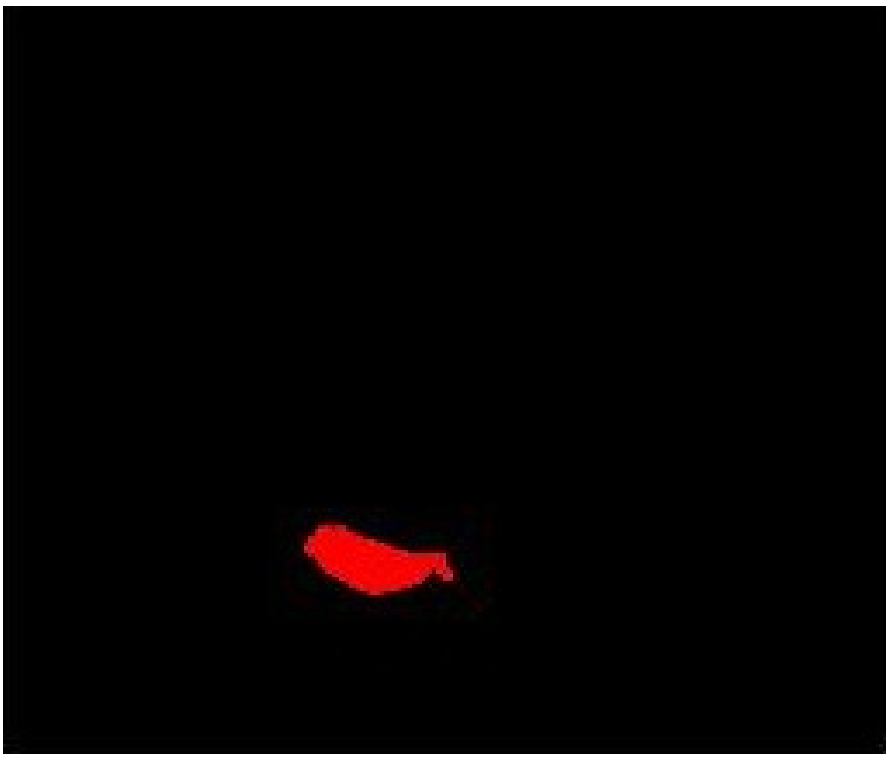

Figure 4.11 Initial segmentation result by region growing using prior information.

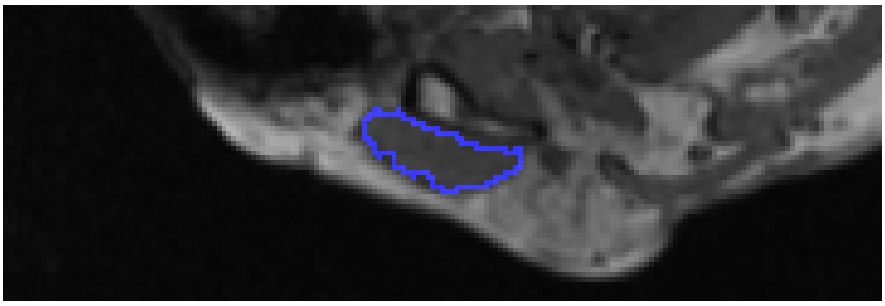

Figure 4.12 Result for the sample image by using method c.

4.5.4. Method d: MRF based segmentation using labeled atlas

The importance of using prior information in medical image segmentation is discussed before. In this section we want to perform a segmentation method based on the maximum likelihood estimation for the MRF models, using prior information. The prior information is in the form of average of labeled atlases and EM algorithm is used for estimation of model parameters.

The method used in this part is like [29] which use probabilistic atlas in MRF-EM segmentation and initialization . Different from MRF-EM model used in [28], in this method, prior probability is not in the form of smoothness term. The prior information is introduced as probabilistic atlas in the expectation step of the EM algorithm as follows:

$$P_{ij}^{t+1} = \frac{G(d_i, \mu_j, \sigma_j) P(f_i = 1 \mid P_{N_i}^t)}{\sum_{k=1}^{2} G(d_i, \mu_k, \sigma_k) P(f_i = k \mid P_{N_i}^t)} \tag{4.4}$$

Here, $P(f_i = 1 \mid P_{N_i}^t)$ is the prior probability that is equal to probabilistic atlas as follows:

$P(f_i = 1 \mid P_{N_i}^t) = P_{i1}^{atlas}$

P_{i1}^{atlas} is the probability of the pixel i to have label 1. The probability is computed by using previously registered and mapped manually segmented train images. This probability is kept constant trough the segmentation.

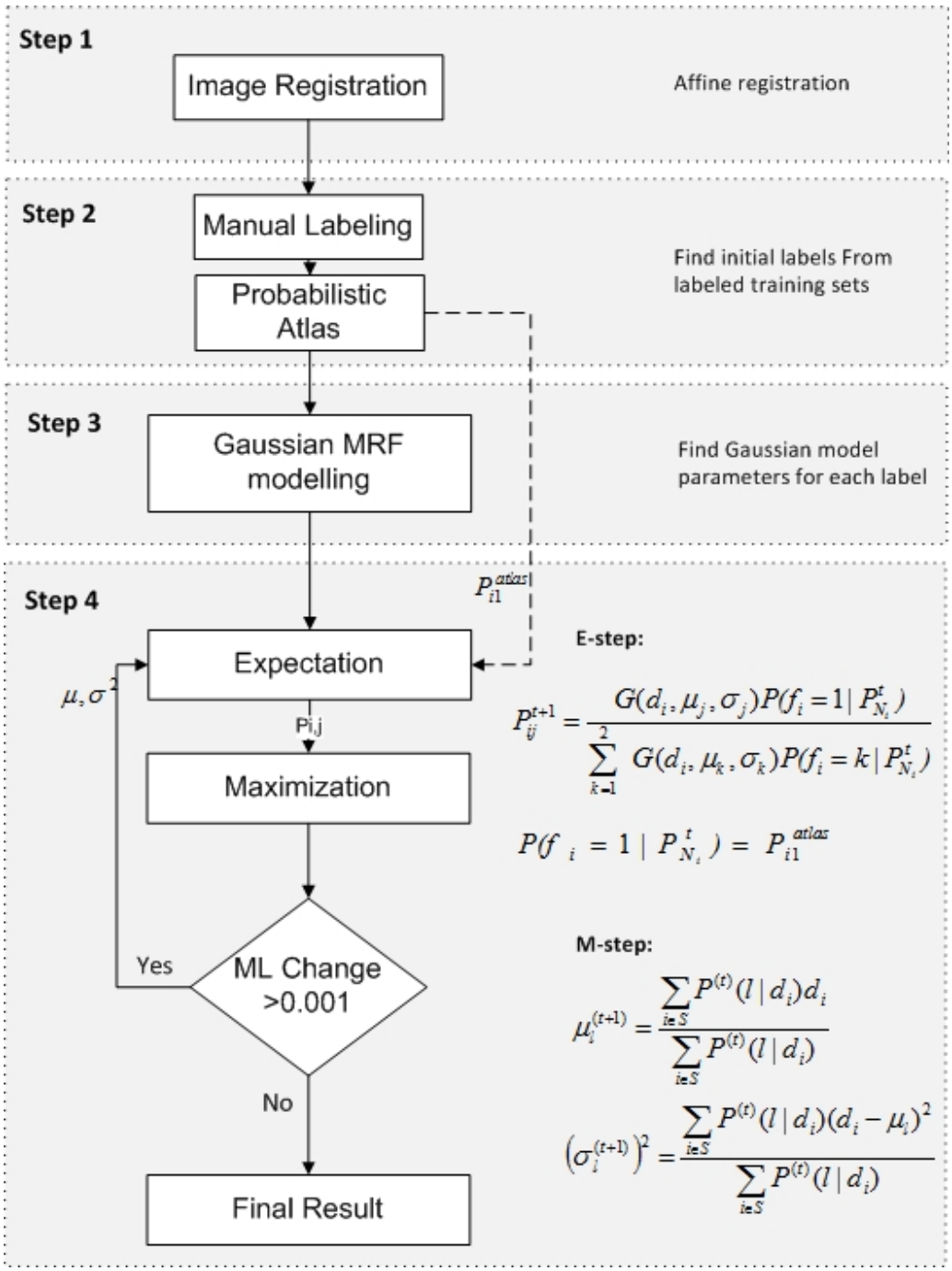

Figure 4.13 Overview of method d.

The method can be summarized in the following steps

Step 1: Image registration: Like the previous methods, an affine registration is applied to the experimental sets in the first step.

Step 2: Manual labeling and Probabilistic atlas: In this step, training sets are segmented manually and the probabilistic atlas is constructed. The constructed atlas is used in expectation step of the EM algorithm as prior information.

By applying the majority voting method the most probable label for each pixel is assigned. This average atlas is a binary image that has value 1 in the pixels that are labeled as the target tissue in more than 4 slices and has value 0 in other pixels. The resulting average atlas is shown in figure 4.14. This atlas is used to construct initial models in step 3.

Step 3: Gaussian MRF modeling: This part is similar to step 3 in section 4.5.2. Initial Gaussian models are estimated from the average atlas from the previous step and initial Gaussian model parameters, μ, σ^2, are computed.

Step 4: Atlas based MRF-EM: Atlas based segmentation process is applied in this step. As you can see in equation 4.4, the only difference between this method and normal MRF-EM is the definition of the prior probability that includes prior information from a probabilistic atlas. The atlas is constructed using labeled training images in step 2. The algorithm iteratively estimate the new labeling and new Gaussian parameters, μ, σ^2, until the likelihood difference becomes very small (less than 0.001).

Manual labeling is used in this method that is so time consuming. Without considering manual segmentation time, the initial labeling process takes 0.1 seconds by using majority voting on previously labeled training images. The MRF-EM segmentation process takes 7 seconds that makes the overall computation time of this method to be 7.1 seconds for each slice. The boundaries of segmentation result for the sample image is shown in blue in figure 4.15.

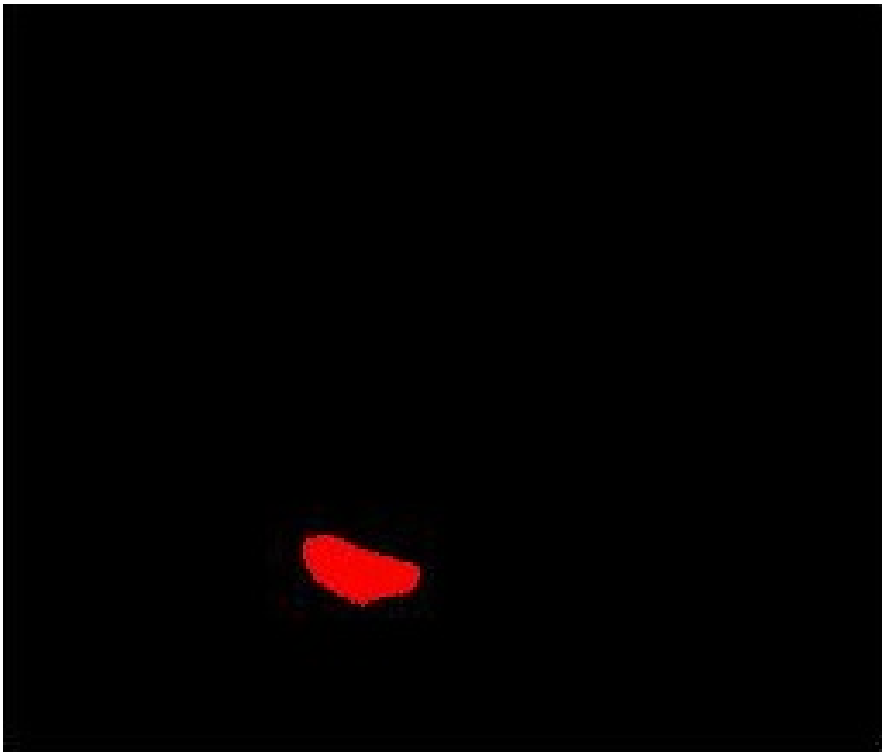

Figure 4.14 Initial segmentation by averaging manually segmented training images.

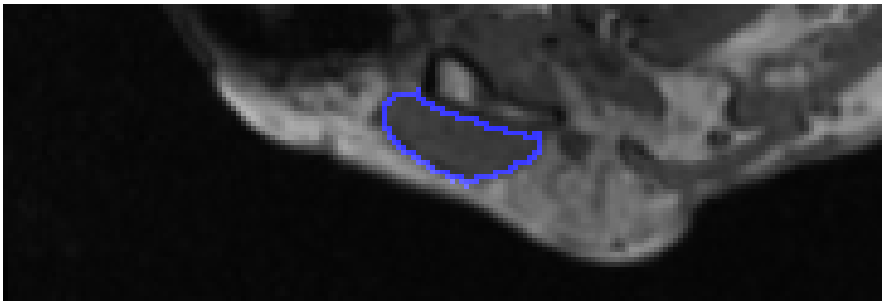

Figure 4.15 Result for the sample image by using method d.

4.5.5. Method e: MRF based segmentation using unlabeled prior information

In the previous sections we performed segmentation processes based on MRF-EM approach with or without using prior information. We also implemented the atlas based segmentation method for the same dataset. All these prior information based methods use atlases that are constructed from manually segmented images. Manual segmentation is a time consuming process especially for 3D segmentation and also decreases the automaticity of the method.

In this method, we try to incorporate the prior information to an MRF model not by using a labeled atlas but by using the original unlabeled images in the training set that can be called as the "latent atlas". Prior information is not used as the initial labeling of the MRF model but is included to the energy function of the MRF model. By doing this, through the EM learning steps, the incorporation of the atlas and the model is updated and learned until convergence. This way of incorporation of many data sets has been considered in [32] where the incorporation is updated at every iteration step of the level set model.

Unlike other methods that perform a MAP estimation to estimate the labeling and use it in pair-wise clique potential computation, we define the prior probability $P(f_i = 1 \mid P_{N_i}^t)$ without using labels. To take advantage of un-labeled training images, we compute the difference between the mean of each class in the current step μ_l and the intensity value of the corresponding pixel i in the neighboring set N_i. We prefer the pixels with less difference to have higher clique potentials so we subtract the difference value from 1. The value 1 is the maximum value that the difference result can take. By performing summation over all training images the overall prior probability for pixel i is computed. The prior probability is defined as:

$$P(f_i = 1 \mid P_{N_i}^t) = 1 - \mid \mu_l - d_{N_i} \mid \tag{4.6}$$

where N_i is the neighboring system defined in section 3.2 that includes training sets and $l \in \{0,1\}$ is the desired label.

By using this feature, the average difference between the target tissue distribution and the training images is computed. Figure 4.16 shows the presentation of V for the sample image. As can be observed from the image, the prior information gives a good estimate of the pixels that may be in the target tissue. This image is like an imaginary image that an specialist doctor may have in her/his mind due to seeing thousands of MRI pictures.

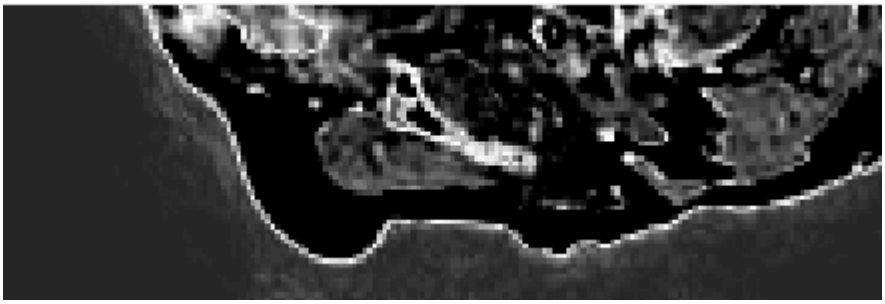

Figure 4.16 Presentation of clique potential for the sample image in one segmentation step.

The important point about this picture is that the target tissue is fully unconnected from the neighboring tissues. This feature helps the segmentation process a lot in the segmentation of FSTs that are generally connected to the neighboring tissues.

An overview of this method is shown in figure 4.17.

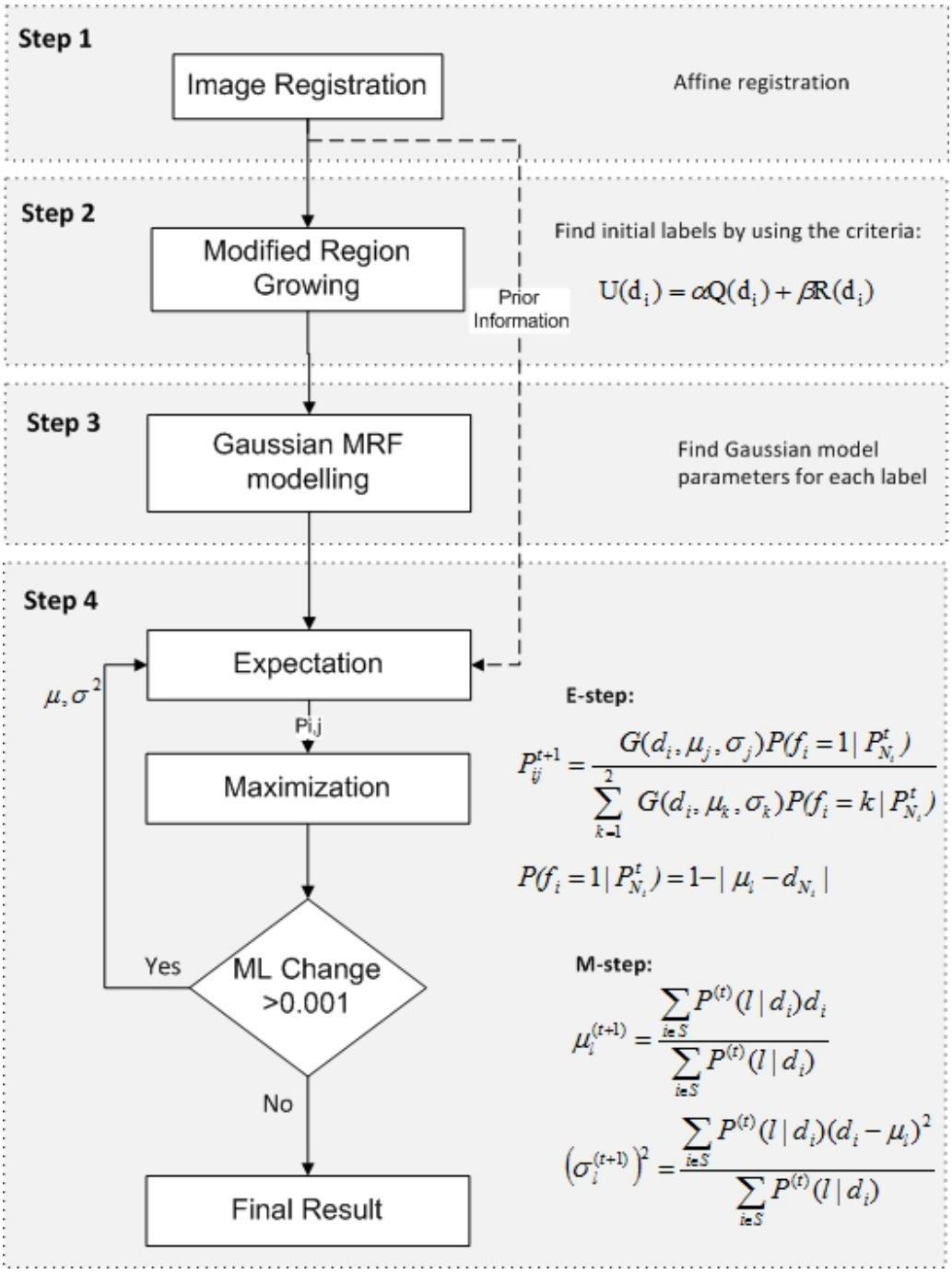

Figure 4.17 Overview of method e.

The important steps in this method are:

Step 1: Image registration: Like the previous methods, an affine registration is applied to the experimental sets in the first step.

Step 2: Modified region growing: In this step, modified region growing algorithm described in part 4.5.3 step 2 is used to estimate the initial segmentation for the proposed MRF based segmentation algorithm. In the modified region growing, not only the pixels in the same slice but also corresponding pixels in the unlabeled training sets are considered. The resulting initial labeling image is just like figure 4.11.

Step 3: Gaussian MRF modeling: This step is similar to step 3 from part 4.5.2. Initial Gaussian models are estimated from the average atlas acquired in the previous step where initial model parameters, μ, σ^2, are computed.

Step 4: MRF-EM based segmentation: In this step, an MRF framework is employed to model intensity distribution of two different classes of labels in the test image. The initial estimate is computed in steps 2 and 3. The energy function is computed by using registered unlabeled train images from step 1. The segmentation process can be summarized in the following steps:

1. Compute the posterior probability

$$P_{ij}^{t+1} = \frac{G(d_i, \mu_j, \sigma_j) P(f_i = 1 \mid P_{N_i}^t)}{\sum_{k=1}^{2} G(d_i, \mu_k, \sigma_k) P(f_i = k \mid P_{N_i}^t)} \tag{4.7}$$

where $G(d_i, \mu_1, \sigma_1)$ is the Gaussian distribution for $l = 1$ in the step t as defined in equation (3.74) and $P(f_i = 1 \mid P_{N_i}^t)$ is the prior probability defined in (4.6) over S.

2. Update the parameters

$$\mu_1^{(t+1)} = \frac{\sum_{i \in S} P^{(t)}(1 \mid d_i) d_i}{\sum_{i \in S} P^{(t)}(1 \mid d_i)} \tag{4.8}$$

$$\left(\sigma_1^{(t+1)}\right)^2 = \frac{\sum_{i \in S} P^{(t)}(1 \mid d_i)(d_i - \mu_1)^2}{\sum_{i \in S} P^{(t)}(1 \mid d_i)} \tag{4.9}$$

3. Compute likelihood difference $|P^t(d_i,\mu_1,\sigma_1)-P^{t-1}(d_i,\mu_1,\sigma_1)|/P^t(d_i,\mu_1,\sigma_1)$. If the difference is bigger than 0.001 go to the step 1 and repeat the process elsewhere end the algorithm.

The initial labeling process takes 2.2 seconds by using the new region growing algorithm. The MRF-EM segmentation process takes 24.3 seconds that makes the overall computation time of this method to be 26.5 seconds for each slice. The result of this segmentation process is shown in figure 4.18. The boundaries of the segmented area are shown in blue.

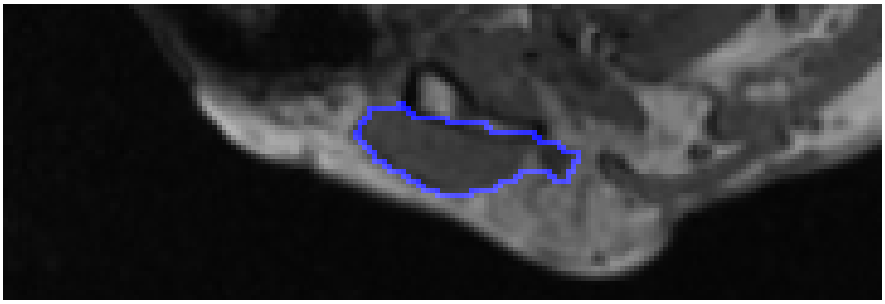

Figure 4.18 Result for the sample image by using method e.

4.6. 3D Segmentation

MRI scans consist of several 2D slices that together construct a 3D image of the interested area. So, when the target tissue is segmented in a single slice, the segmentation process can proceed through other neighboring slices so that the 3D shape of the whole tissue can be extracted. In this section, we want to perform 3D segmentation by applying our proposed 2D segmentation method on each slice successively but using some additional processes.

The experiment is applied to 10 MRI sets. Each time, one of them is selected as the target set while the other 9 sets are considered as the training sets. The starting and ending slices in a set are determined by the operator before the process begins.

The segmentation algorithm for the new slices is the same as in the 2D segmentation. However, there are two initial values that the region growing algorithm starts with: seed point and threshold. In 2D segmentation, these values are set by the user. In 3D segmentation, these values are set by the user only for the first slice and then for the new slices some additional processing blocks are added to estimate these values automatically using the information in the previous slice and the current slice.

After setting the threshold and the seed point, no manual interaction is needed for segmentation and the process continues automatically until the last slice is segmented. The overview of the 3D segmentation system is shown in figure 4.19.

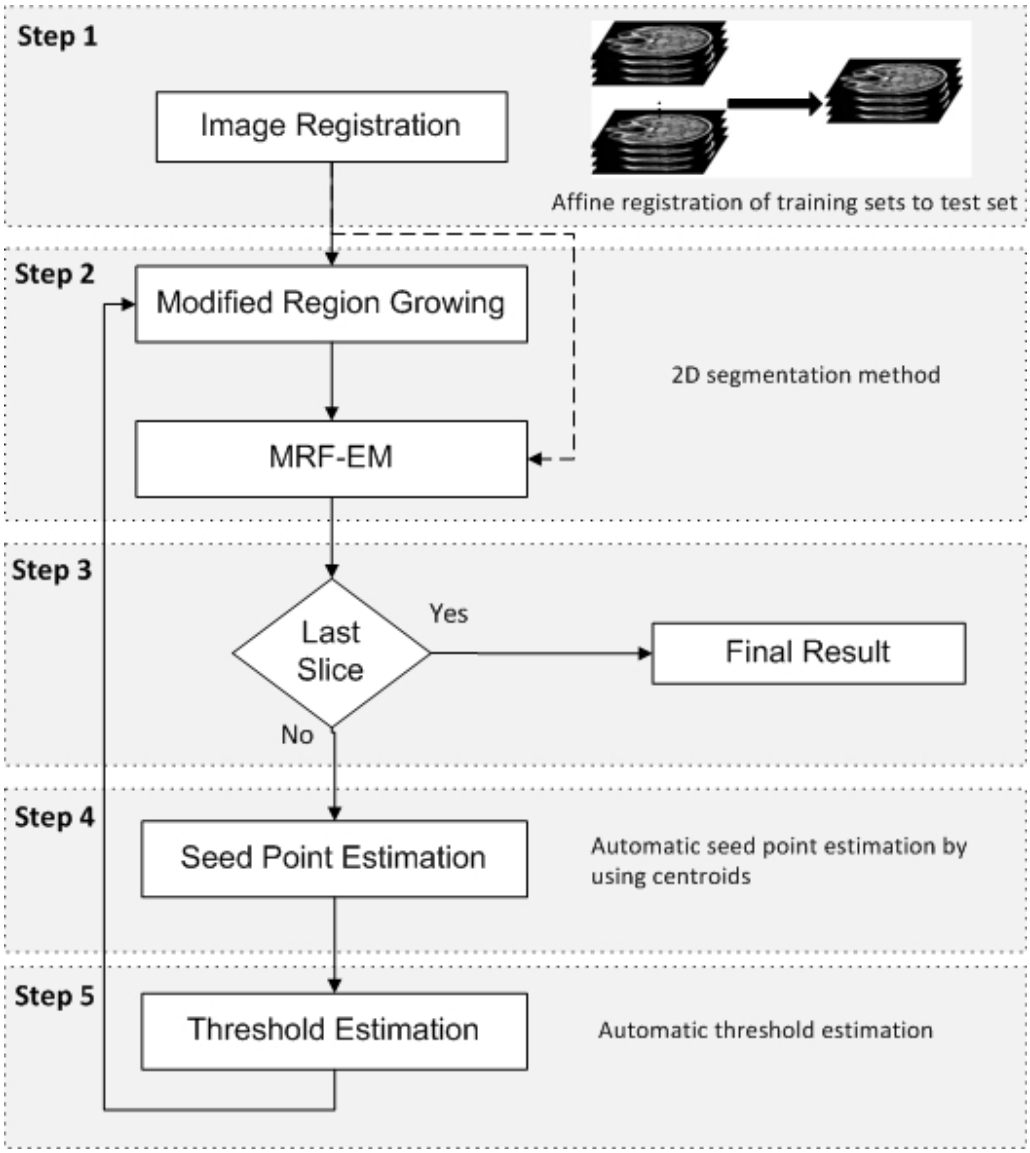

Figure 4.19 Overview of 3D segmentation method

The 3D segmentation process is summarized in the following steps:

Step 1:Image registration: All ten image sets are registered by affine registration. The registration process is like in the 2D method.

Step 2: 2D segmentation: The segmentation method proposed in Section 4.5.5 is implemented in this step. The region growing algorithm starts from the seed point

and uses the threshold set by the user for the first slice. The seed points and the threshold values for the successive slices are estimated in steps 4 and 5. Here, registered images are used to perform region growing where they are also used as the prior information in MRF-EM method. The result of this block is a segmented 2D binary image.

Step 3: Decision making: In this step, algorithm checks if this is the last slice to be segmented or there are other slices left. It ends the segmentation in the first case and in the other case it proceeds to seed point and threshold estimation blocks to estimate these values for the successive slice and starts segmentation in the new slices. The starting and ending slices are set by the user at the very beginning.

Step 4: Seed point estimation: In this step, the new seed point for the segmentation of the next slice is estimated. To find the location of the new seed point, we assumed that the centroid of the previous segmented area coincides with the target area of the new slice. Because of the anatomy of the target tissues and also the resolution of the MRI images this is a realistic assumption and the centroid lays in the target area for almost all cases.

However, because of the special characteristics of the FST texture, having a high intensity in-homogeneity, the centroid may coincide with one of these in-homogeneities and this halts the region growing. There may be several white points with high intensity in the tissue that corresponds to fats inside the muscle. When the region growing algorithm starts from that point, the process wouldn't be able to join the neighboring pixels due to the wrong initial estimate.

To avoid this problem, 8 other seed point candidates were selected as alternatives for the centroid. We define 8 extreme points for the previously segmented region as top left, top right, left top, right top, left bottom, right bottom, bottom left and bottom right. Then the new seed point candidates are selected on the lines between the centroid and the 8 extreme points in the region as shown in figure 4.20. When the estimated seed point intensity is abnormal compared to the intensity model of the previous slice, the new seed point was selected from the candidates. The intensity value of the new candidate is also

checked to be close to the intensity model. Then the process is continued by using the candidate as the seed point.

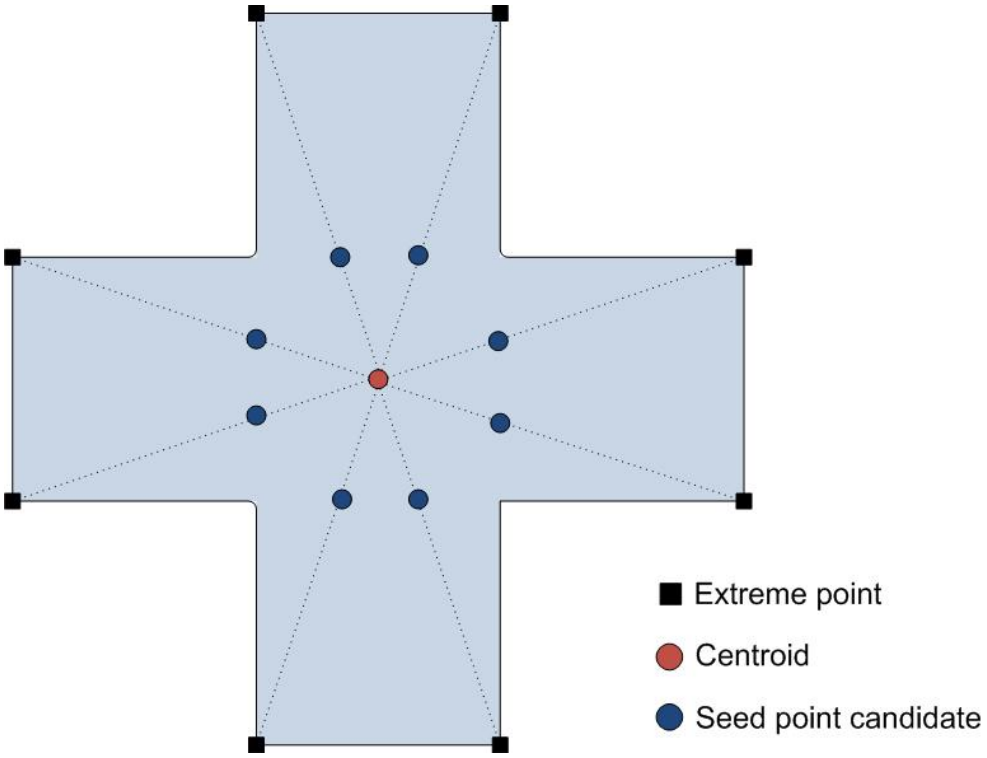

Figure 4.20 Seed point estimation candidates. Extreme points are shown in black, centroid is shown in red and the new candidates are shown in blue.

Step 5: new threshold estimation: The region growing algorithm needs another input to start and that is the threshold value. The algorithm checks the difference between the energy function of the new pixel and the region mean, with this criterion. We use a learning algorithm to estimate the new threshold value. The energy values assigned to all pixels in the already segmented region are used in this learning method. The standard deviation of these values are computed and selected as the threshold value for the new slice. Since the slices are normalized by a bias field correction algorithm, the tissue intensity distribution is so close for two neighboring slices that makes this estimation value promising.

A simple interpolation is used to construct 3D shape of the target tissues from 2D slices. The acquired models for the masseter and temporalis muscles are shown in figure 4.21 and 4.22.

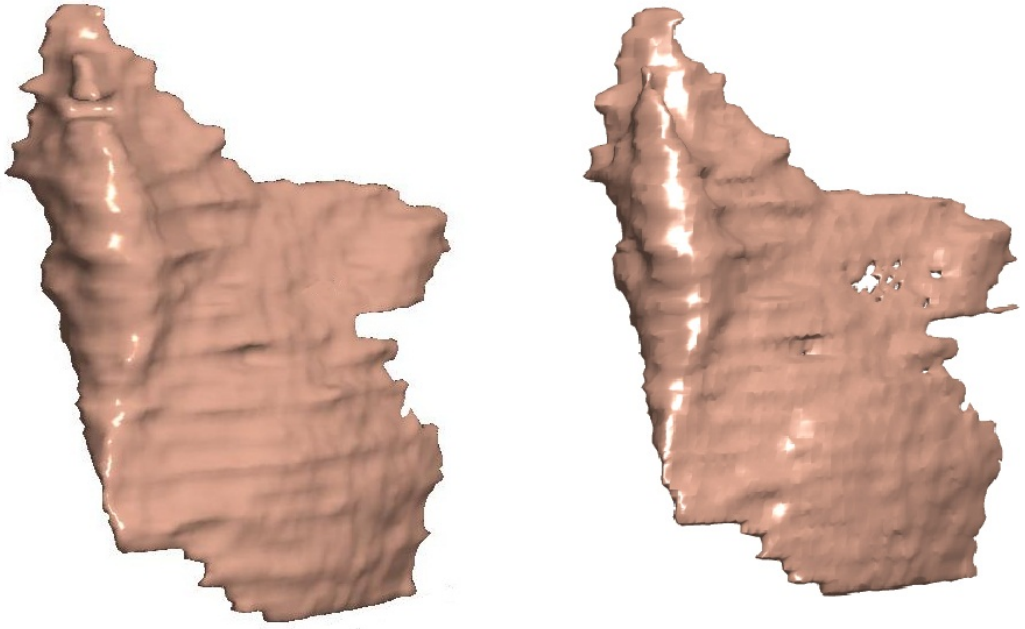

Figure 4.21 3D segmentation result for temporalis. a. Manual segmentation result, b. Segmentation result our method.

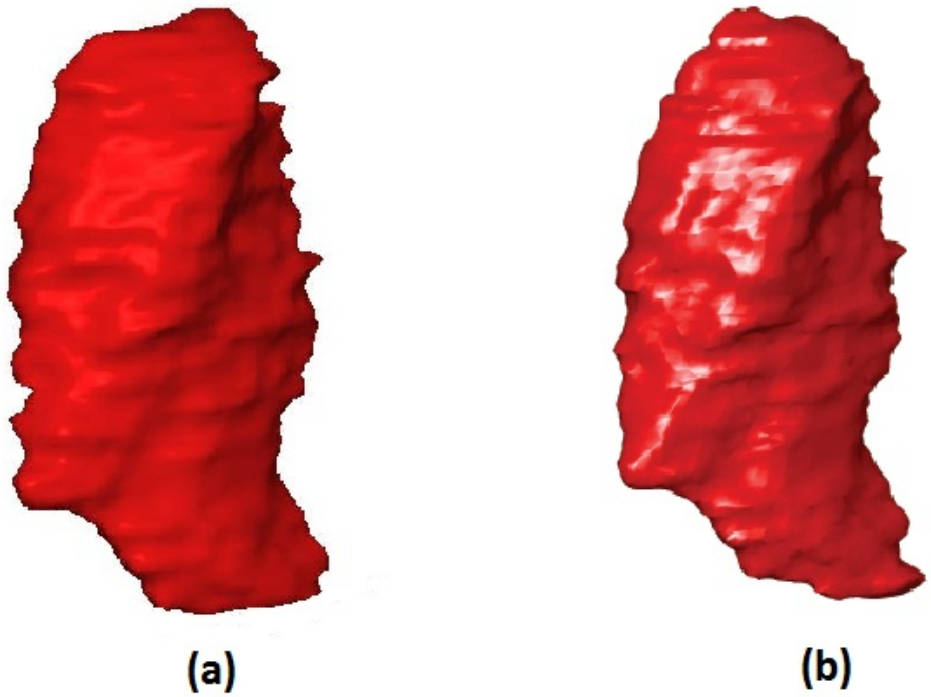

Figure 4.22 3D segmentation result for masseter. a. Manual segmentation result, b. Segmentation result our method.

CHAPTER 5

RESULTS AND DISCUSSION

5.1. Validation

There are a few studies related to facial soft tissue segmentation and they do not include a qualitative evaluation since there is no ground truth available for these tissues. The validation of our segmentation method was done by comparing the automatic segmentation results with the manual segmentation results. For this purpose, every target tissue is segmented manually in all slices that it appears. This process is repeated for all 10 experimental sets and these manual segmentations are only used as the ground truth. More than 2700 slices are segmented manually to construct the ground truth. The manual segmentation is done by taking "3D Anatomy for Otolaryngology & Head & Neck Surgery"[64] software as reference and under the supervision of an expert.

We used dice metric κ [65] to evaluate the correspondence between the segmentation result and the ground truth. The metric is defined as follows:

$$\kappa = 2 \times \frac{S \cap T}{S + T} \times 100\% \tag{5.1}$$

where S is the segmented area and T is the ground truth.

5.2. 2D segmentation accuracy

We performed 2D segmentation to label masseter muscle in one MRI slice with 5 different methods. In this part we will see the accuracy of each method using dice metric. We will discuss the advantages and disadvantages of each method.

5.2.1. Method a: Atlas based segmentation

Atlas based segmentation is known to be successful in brain tissue classification but as you can see in table 5.1 and figure 5.1 , the results are not very good for the masseter tissue. Human brain's shape is mostly similar in different individuals but facial tissues like masseter may have various shapes in different people. This method completely depends on the atlas and when the shape and position of the tissue of the atlas are different from the shape and position of the tissue of the test data then the registration may result in wrong answer. The shape of the head and face are also very affective in the registration process.

As you can see in table 5.1, the segmentation result is very poor for set 4 due to the difference between the tissue and head shapes of the atlas and the data set 4. If we exclude set 4, the average accuracy is increased about 5% and becomes 77.66 %. This problem can be solved either by selecting the experimental data similar to the atlas or by increasing the number of training images in a way that covers all the possible shapes. Also, some supervised methods can be used to avoid wrong registrations.

This method is simple to implement but the non-rigid registration process and atlas construction are time consuming. There is also a lot of human interaction in this method because of manual labeling.

Table 5.1 Accuracy results for method a.

Set	Set 1	Set 2	Set 3	Set 4	Set 5	Set 6	Set 7	Set 8	Set 9	Set 10	Average
Accuracy	66.66	83.23	76.72	30.24	84.75	60.98	81.97	82.16	83.35	79.13	72.92

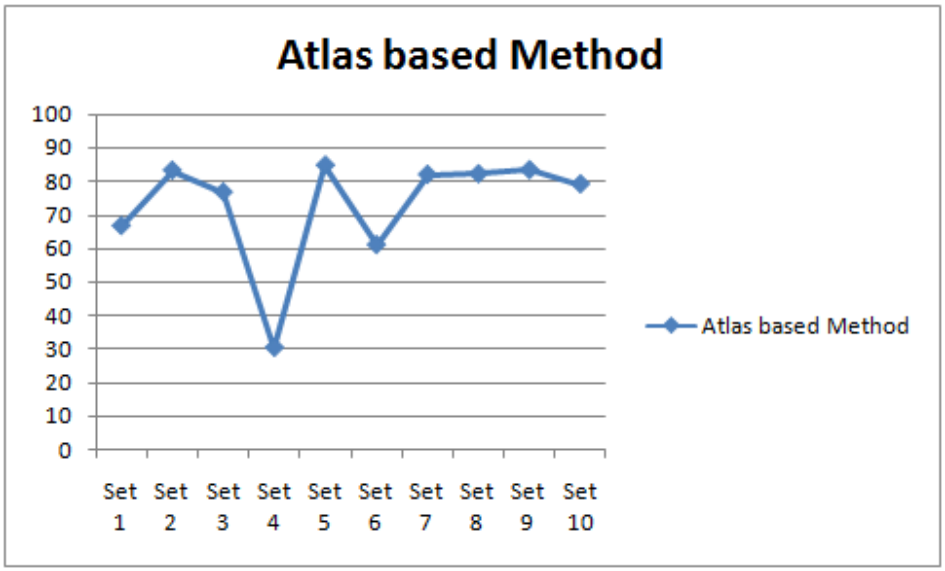

Figure 5.1 Accuracy results for 10 slices using method a.

5.2.2. Method b: MRF based segmentation with initials from region growing algorithm

The important concepts in MRF-EM based segmentation are defining a proper MRF model that fits the observed data and setting an appropriate initial estimation. The region growing algorithm is used to perform initial labeling in this method. Prior information from training sets is totally ignored in this method to see the influence of it on segmentation accuracy. Only a single point is marked on the tissue to be segmented.

The accuracy results are shown in table 5.2 and figure 5.2. The segmentation is very successful in most cases, such as sets 1,2,3,8, but in some cases, such as sets 4 and 5, segmentation results are poor.

Table 5.2 Accuracy results for method b.

Set	Set 1	Set 2	Set 3	Set 4	Set 5	Set 6	Set 7	Set 8	Set 9	Set 10	Average
Accuracy	88.24	86.12	88.01	49.92	19.34	75.3	68.97	92.65	82.4	68.25	71.92

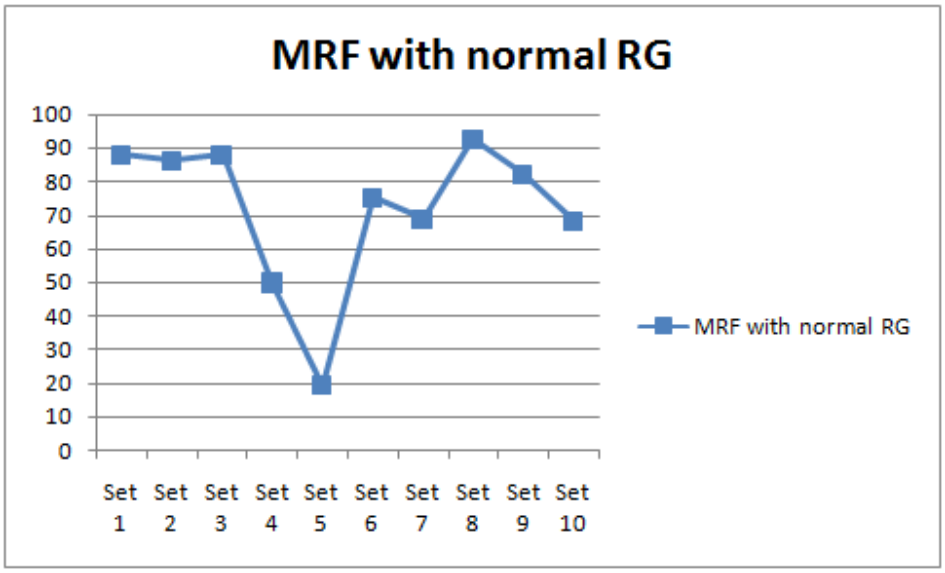

Figure 5.2 Accuracy results for 10 slices using method b.

To investigate this issue, we checked the initial labeling for the worst result (i.e., set 5) and the best result (i.e., set 8). The region growing outcome for set 5 and 8 are shown on the original image in figure 5.3. As you can see, the initial labeling is so poor in case of set 5 that ends in poor overall segmentation where case 8 starts with a good estimate and results in more than 92% accuracy.

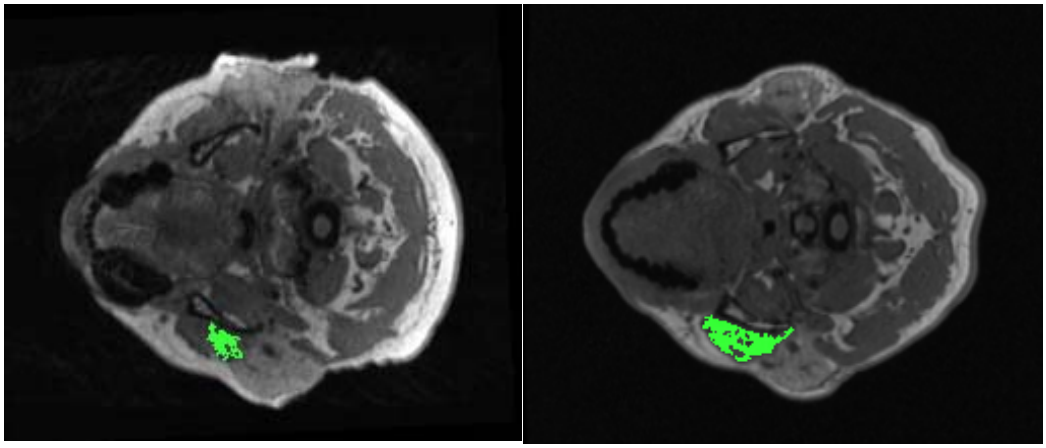

Figure 5.3 Left. Initial labeling for the worst case (set 5) Right. Initial labeling for the best case (set 8).

The only input information that we used in this method is the intensity values of the current slice. So, the region growing or MRF-EM algorithms may add neighbor tissues with similar intensity or may exclude some parts of the tissue because of intensity dissimilarity.

5.2.3. Method c: MRF based segmentation with initials from region growing algorithm using prior information

In this experiment, we tried to solve the problem of initial labeling where a modified region growing algorithm was used for initialization. As you see in table 5.3 and figure 5.4, there is about 12% improvement in the segmentation accuracy. This emphasis the importance of initial labeling in MRF-EM segmentation and also using prior information in region growing algorithm. The prior information used here is unlabeled raw training images.

Although there is an overall improvement in the segmentation performance, in some cases accuracy decreases. For example, for previously investigated sets 5 and 8, although the accuracy is improved about 59% for set 5, there is about 17% decrease for set 8.

Table 5.3 Accuracy results for method c.

Set	Set 1	Set 2	Set 3	Set 4	Set 5	Set 6	Set 7	Set 8	Set 9	Set 10	Average
Accuracy	86.87	93.33	84.18	82.86	78.9	77.56	74.38	75.68	90.71	92.89	83.74

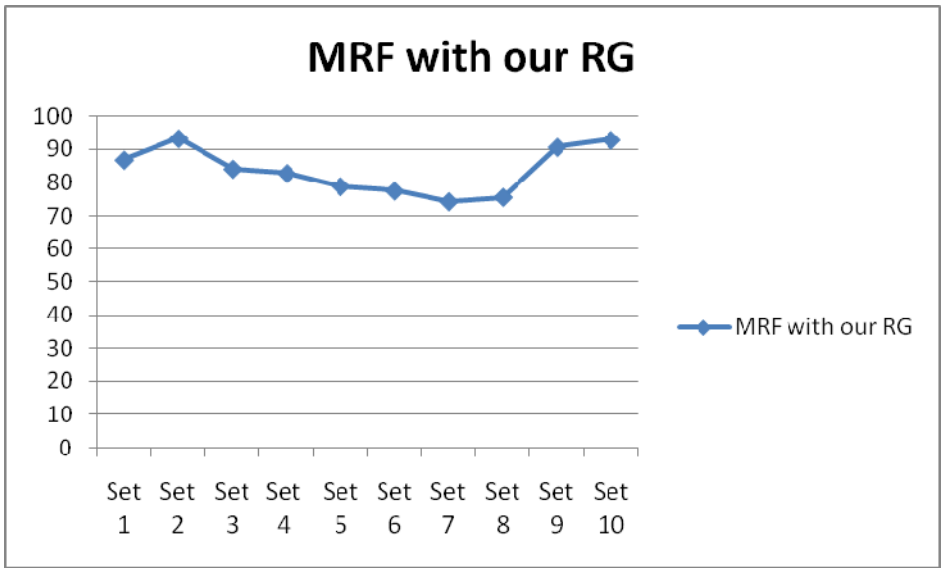

Figure 5.4 Accuracy results for 10 slices using method c.

The initial labeling with modified RG for sets 5 and 8 are shown in figure 5.5. The improvement in set 5 and decrement in set 8 are very clearly observed. The prior information brings improvement for set 5 where there is an intensity in-homogeneity but it is not useful for set 8, which has a shape different than the training sets. However the overall improvement is noticeable and there isn't any big decline for different cases as can be seen in figure 5.4.

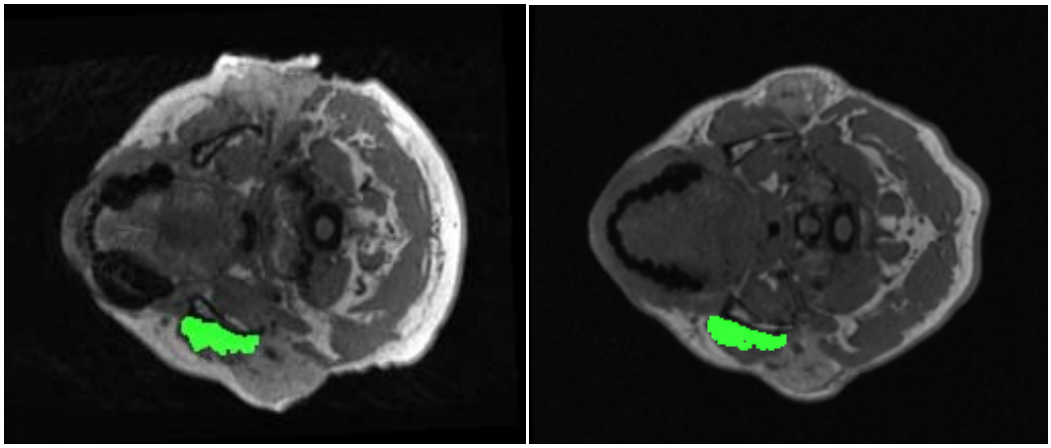

Figure 5.5 Left. Initial labeling for set 5 Right. Initial labeling for set 8.

In this kind of segmentation methods, keeping the balance between the intensity information and the prior information is an important issue. Another important concept in using the prior information in the RG algorithm is that the resulting segmented regions are continuous and smooth, as can be seen in figure 5.5. We want to mention once more that the MRF-EM process for this method is the same as the previous one and the improvement is only because of initial labeling which includes prior information.

5.2.4. Method d: MRF based segmentation using labeled atlas

The accuracy results for this method is shown in table 5.4 and figure 5.6. Here, labeled training images are selected as prior information. Also initial estimation is derived from the labeled training sets. The initial labeling is the same for all images. Although this constant labeling makes the method so simple and fast, it may cause some wrong estimation in the beginning.

As you can see in table 5.4 the segmentation performance is close to the MRF based segmentation with modified region growing method (Method c) but it is about 1% lower. Despite the large amount of manual interaction required for the prior information in MRF-EM part, this method shows lower accuracy than the previous method. This is mostly because of the initial estimation.

Table 5.4 Accuracy results for method d.

Set	Set 1	Set 2	Set 3	Set 4	Set 5	Set 6	Set 7	Set 8	Set 9	Set 10	Average
Accuracy	86.98	93.37	71.56	82.68	84.16	59.88	71.89	89.14	94.69	91.05	82.54

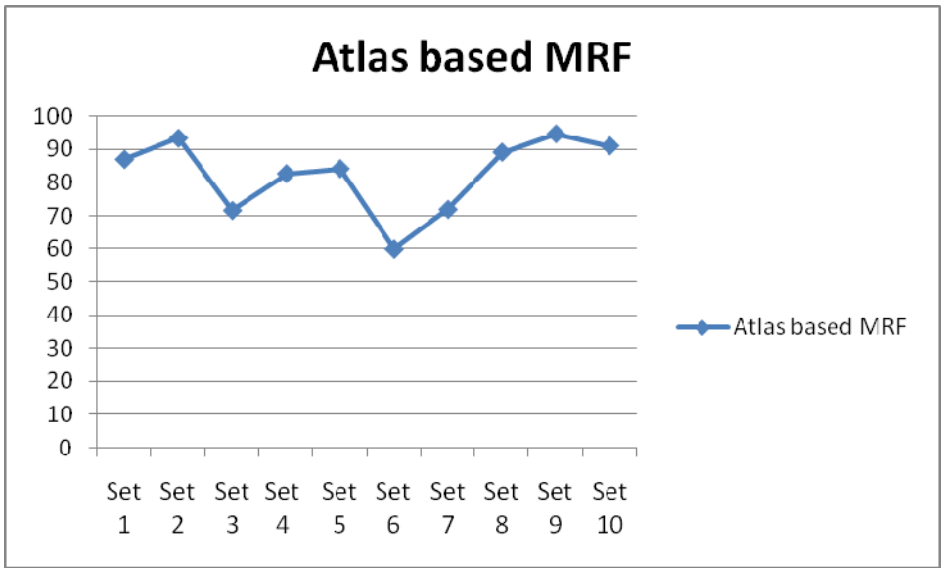

Figure 5.6 Accuracy results for 10 slices using method d.

5.2.5. Method e: MRF based segmentation using unlabeled prior information

Finally, we want to discuss the results of our proposed method for masseter segmentation. The accuracy values are shown in table 5.5 and figure 5.7. This method shows the best overall performance among all tested methods. In 6 out of ten slices, the accuracy of this method is over 90%. The worst results are for sets 6 and 7 which also cause poor results by using normal EM-MRF method (Method c) in part 4.5.3. So we can conclude that, poor initialization is the problem for these cases. But this comment is not true for other low accuracies for sets 2 and 4.

The main problem is in finding a generic solution that results in a good accuracy for all of the images. But this requires that the training set should be big enough to overlap all possible shapes. Another problem is due to the affine registration which also may sometimes cause poor initialization.

However this method has acceptable overall accuracy for masseter tissue. It is important to note that these results are achieved without using any manual segmentation. The only manual interaction is the selection of a seed point and a threshold for region growing algorithm. The threshold value is kept constant because of the previousely applied histogram equalization algorithm. The rest of the method is fully automatic.

Table 5.5 Accuracy results for method e.

Set	Set 1	Set 2	Set 3	Set 4	Set 5	Set 6	Set 7	Set 8	Set 9	Set 10	Average
Accuracy	93.07	83.74	90.03	78.39	90.67	77.23	66.49	93.4	96.11	96.07	86.52

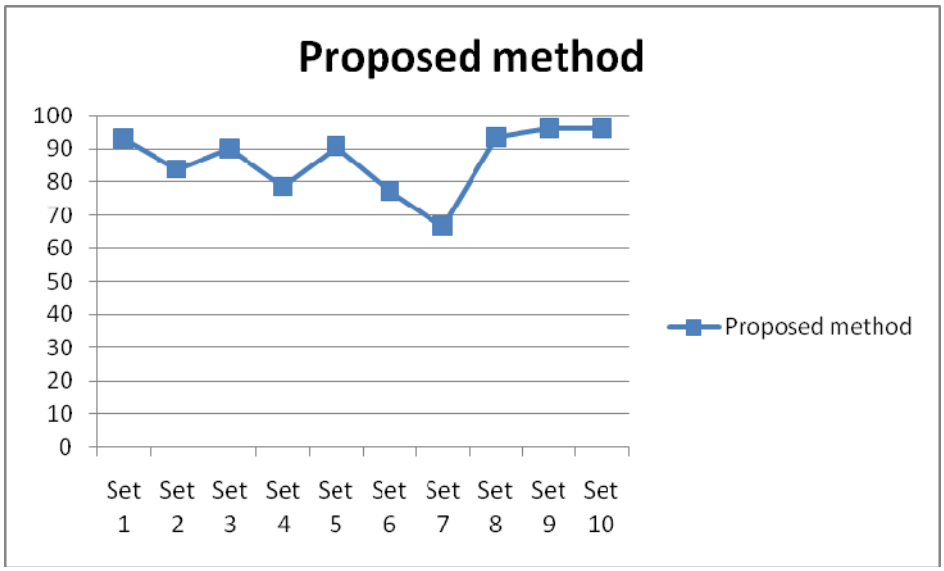

Figure 5.7 Accuracy results for 10 slices using method e.

5.3. Overall 2D results

The results of 2D segmentation for different methods are shown together in table 5.6, figure 5.8 and figure 5.9 for better visualization.

Table 5.6 Overall accuracy results for all methods.

Set	Atlas based Method	Atlas based MRF	MRF with normal RG	MRF with our RG	Our Method
Set 1	66.66	86.98	88.24	86.87	**93.07**
Set 2	83.23	**93.37**	86.12	93.33	83.74
Set 3	76.72	71.56	88.01	84.18	**90.03**
Set 4	30.24	82.68	49.92	**82.86**	78.39
Set 5	84.75	84.16	19.34	78.9	**90.67**
Set 6	60.98	59.88	75.3	**77.56**	77.23
Set 7	**81.97**	71.89	68.97	74.38	66.49
Set 8	82.16	89.14	92.65	75.68	**93.4**
Set 9	83.35	94.69	82.4	90.71	**96.11**
Set 10	79.13	91.05	68.25	92.89	**96.07**
Average	72.92	82.54	71.92	83.74	**86.52**

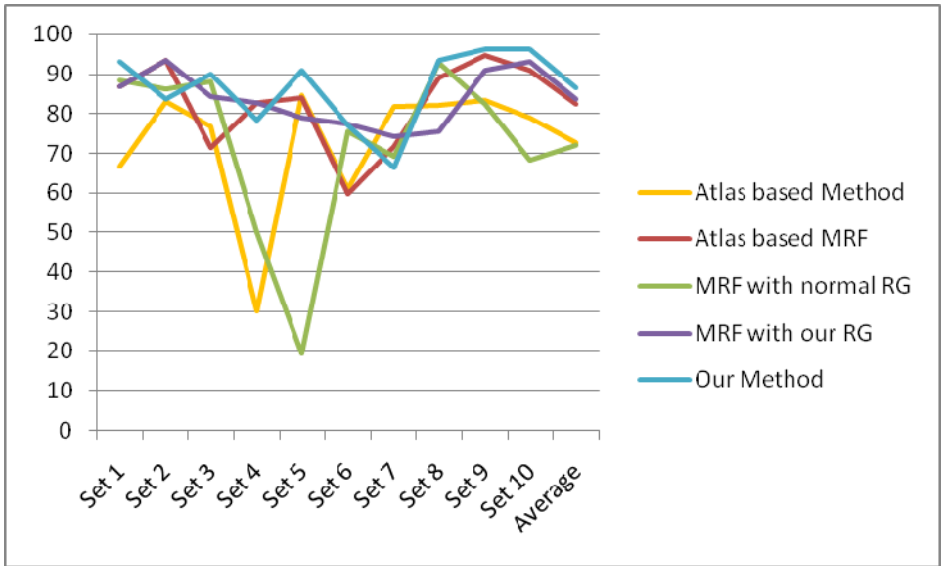

Figure 5.8 Accuracy results using 5 different methods.

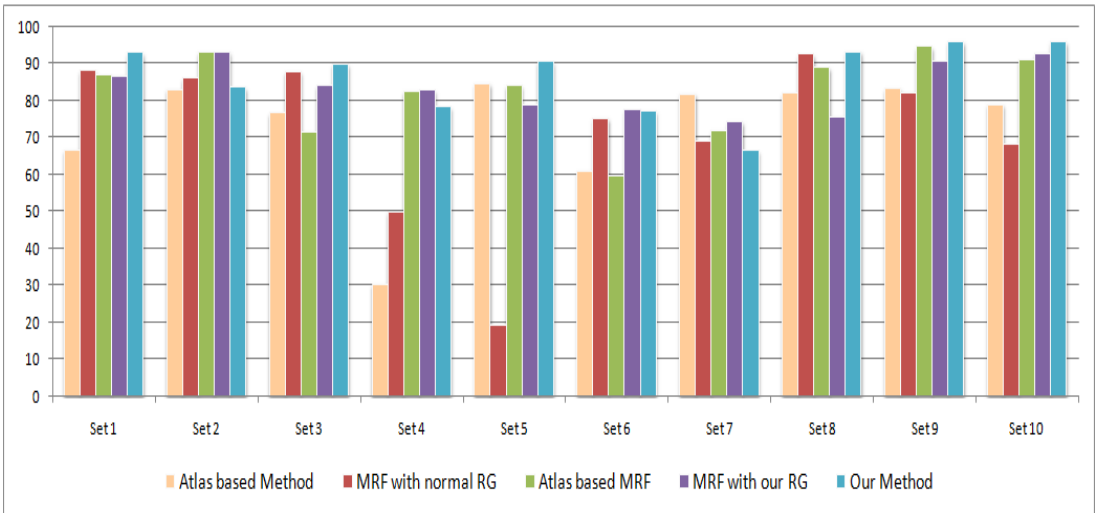

Figure 5.9 Comparison of accuracy between different methods.

5.4. 3D segmentation results

The same dice metric is used for performance evaluation as in equation 5.1. In this section, the metric measure is evaluated by comparing volumes of the segmented tissues and the ground truth. The results for the target tissues are shown in table 5.7. The average accuracy of masseter is higher than temporalis tissue. This is because of the uncommon shape of the temporalis muscle in most of the slices whereas masseter usually has a simpler shape.

Table 5.7 3D segmentation accuracy results for 4 different tissues.

Set	left temporalis	right temporalis	left masseter	right masseter	Average
Set 1	80.63	83.56	89.35	88.84	**85.595**
Set 2	71.5	81.39	82.07	82.8	**79.44**
Set 3	84.9	84.35	90.3	88.36	**86.9775**
Set 4	78.2	76.28	77.37	78.93	**77.695**
Set 5	85.87	83.85	80.22	84.86	**83.7**
Set 6	80.84	82.19	81.95	83.07	**82.0125**
Set 7	82.25	81.6	85.61	80.15	**82.4025**
Set 8	84.4	84.27	84.64	86.18	**84.8725**
Set 9	84.62	86.98	88.98	87.01	**86.8975**
Set 10	81.52	78.74	82.64	88.73	**82.9075**
Average	**81.473**	**82.321**	**84.313**	**84.893**	

A chart of the 3D segmentation results is shown in figure 5.10. The accuracies of different tissues are related to each other according to the chart. So a set with higher masseter accuracy usually has a higher accuracy in temporalis also.

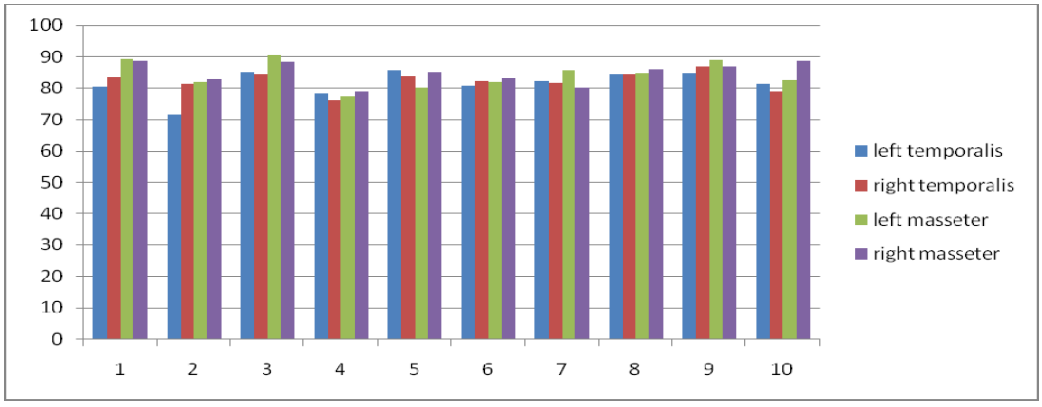

Figure 5.10 3D segmentation accuracy results for 10 different sets.

CHAPTER 6

CONCLUSION

6.1. Conclusion

In this study, we tested four different state of the art methods for 2D facial soft tissue segmentation on magnetic resonance images. These methods are: Atlas based segmentation (Method a), MRF based segmentation with initials from region growing algorithm (Method b), MRF based segmentation with initials from region growing algorithm using unlabeled atlas (Method c), MRF based segmentation using labeled atlas (Method d).

We then proposed a new segmentation method named MRF based segmentation using unlabeled prior information (Method e).

Our main interest in this work was to investigate the role of prior information in FST segmentation by using different methods. We applied all these methods on 10 different MRI slices belonging to different individuals and aimed to segment the masseter muscle in them. The experimental MRI sets were registered 3 dimensionally before the segmentation so the slices corresponded to each other.

Method a is fully based on registration of labeled training images to the test image. The average accuracy of this method for 10 different sets is 72.92%. In the second method (Method b), an MRF-EM based segmentation method with initials from region growing is applied to perform the same work. No prior information is

used in this method and the acquired average accuracy is 71.92 %. Although the first method uses labeled prior information, the accuracy of the second method is very close to the first one. This shows that atlas based methods are not as successful as expected in segmentation of FSTs. The most important reasons for this failure are the variation of the tissue shape among the sets and the existence of similar tissues in the neighborhood of the target tissue.

Method c is similar to Method b, except the fact that the region growing algorithm is improved in a way that it uses prior information in Method c. The accuracy is improved to 83.74 % which emphasizes the importance of initial estimate in MRF-EM process and also the importance of using prior information in initialization.

In Method d, the similar MRF-EM framework is used but this time the labeled training images are implemented in segmentation and also in initial model estimation. The method reaches 82.54% accuracy that is close to Method d which doesn't use manual labeling. We may conclude that determining the target tissue with a seed point and a threshold (like we did in Method c) is more informative for MRF-EM framework than labeled atlases.

In the end, we proposed a method that uses unlabeled prior information both in initial estimation and during MRF-EM optimization. This method is just like an experienced anatomist's segmenting a tissue. While he is trying to segment a tissue, he uses all of his past experiences of observing many similar data, although they were not segmented. The average accuracy for this method is 86.52% which is better than the performance of Method d that requires extra manual labeling. The proposed method starts from the same initial estimates as Method c but it uses prior information inside the MRF-EM process that causes about 4% improvement in the final segmentation accuracy. The importance of using prior information can be shown better when we compare Method b with our proposed method where using prior information causes about 15% improvement.

Finally, we used the proposed 2D segmentation method to perform 3D segmentation of 4 different facial soft tissues in 10 MRI sets. The sets are segmented slice by slice with some additional tasks such as seed point and threshold

estimations for the successive slices. The segmentation process could also be performed three dimensionally but it increases the complexity of the problem. This method achieved 81.47% and 82.32% accuracy results for right and left temporalis respectively and 84.31% and 84.89% for right and left masseter respectively. Considering the difficulties of 3D segmentation, these results seem to be acceptable for FST segmentation.

6.2. Future work

In the current work, we introduced an MRF framework that includes prior information in tissue modeling. This is like a network where the training sets are connected to the test set and have affect on it. In the future, we aim to add some other information to this network to improve the learning algorithm and make the system more similar to a decision making system in a specialist's brain. These additional information can be anatomical such as "every muscle is connected to bone", can be morphological, "a bigger head has bigger muscles", or it can be based on biomechanical interactions between the tissues.

We also want to improve the mathematical aspects of defining the problem and the model that fits the desired network.

The registration was a serious problem in the current work in most of the unsuccessful segmentations. The registration process needs to be improved. It can be changed according to the characteristics of the test images.

The main difficulty of this work was the lack of high resolution, full head MRI sets. We believe that existence of high quality images will improve the segmentation performance. A common project with a hospital or clinical institute is considered to be beneficial for this purpose.

REFERENCES

1. G.M. Bydder,M.E. Farrugiaa,J.M. Francis, M.D. Robson, Magnetic resonance imaging of facial muscles. Clinical Radiology, 2007. 62(11): p. 1078-1086

2. J.J. Xia,J. Gateno,J. Teichgraebe,A. Christensen,R. Lasky,J. Lemoine,M. Liebschner, Accuracy of the Computer-Aided SurgicalSimulation (CASS) System in the Treatment of Patients With Complex Craniomaxillofacial Deformity: A Pilot Study. Journal of Oral and Maxillofacial Surgery, 2007. 65(2): p. 248-254

3. I. Ulusoy,E. Akagunduz,F. Sabuncuoglu,O. Ucok S. Gorgulu, Use of the Dynamic Volume Spline Method to Predict Facial Soft Tissue Changes Associated with Orthognathic Surgery. Oral Surgery, Oral Medicine, Oral Pathology, Oral Radiology, and Endodontology, 2010. 110(5): p. e17-e23

4. P.K. Sahoo,S.Soltani,A.K.C. Wong, A survey of thresholding techniques. Computer Vision Graphics and Image Processing, 1988. 41(2): p. 233-260.

5. F. Klawonn,F. Hoppner,R. Kruse,T. Runkler, Fuzzy cluster analysis. 1999: Wiley Interscience.

6. R. Pandiyarajan,S. Ramathilagam,A. Sathya, R. Devi,S. R. Kannan, Modified fuzzy c-means algorithm for segmentation of T1-T2-weighted brain MRI. Journal of Computational and Applied Mathematics, 2011. 235(6): p. 1578-1586.

7. A. Sathya,S. R. Kannan,S. Ramathilagam, Effective fuzzy clustering techniques for segmentation of breast MRI. Soft computing - a fusion of foundations, methodologies and applications, 2011. 15(3): p. 483-491.

8. X. Papademetris,Y. Zhu,A.J. Sinusas,J.S. Duncan, Segmentation of the left ventricle from cardiac MR images using a subject-specific dynamical model. IEEE transactions on medical imaging, 2010. 29(3): p. 668-687.

9. D.E. Oliva R.A. Isoardi, G. Mato, Maximum Evidence Method for classification of brain tissues in MRI. Pattern Recogn. Lett., 2011. 32(1): p. 12-18.

10. T. Rohlfing,R. Brandt,R. Menzel, D.B. Russakoff,C.R. Maurer, Quo Vadis, Atlas-Based Segmentation?, in handbook of biomedical image analysis. 2005. p. 435-486.

11. M. Altaye,S.K. Holland,M. Wilke,C. Gaser., Infant brain probability templates for MRI segmentation and normalization. Neuroimage, 2008. 43(4): p. 721-730.

12. P. Aljabar,R.A. Heckemann,A. Hammers,J.V. Hajnal,D. Rueckert, Multi-atlas based segmentation of brain images: Atlas selection and its effect on accuracy. Neuroimage, 2009. 46(3): p. 726-738.

13. M. Lorenzo-Valdés,G.I. Sanchez-Ortiz,A.G. Elkington,R.H. Mohiaddin,D. Rueckert, Segmentation of 4D cardiac MR images using a probabilistic atlas and the EM algorithm. Medical Image Analysis, 2004. 8(3): p. 255-65.

14. E.M.V. Rikxoort,I. Isgum,Y. Arzhaeva,M. Staring,S. Klein,M.A. Viergever,J.P. Pluim,B.V. Ginneken, Adaptive local multi-atlas segmentation: application to the heart and the caudate nucleus. Medical Image Analysis, 2010. 14(1): p. 39-49.

15. E.M.V. Rikxoort,M. Prokop,B. de Hoop,M.A. Viergever,J.P. Pluim,B.V.Ginneken, Automatic segmentation of pulmonary lobes robust against incomplete fissures. IEEE Transactions on Medical Imaging, 2010. 29(6): p. 1286-1296.

16. A. Akselrod-ballin,M. Galun,J. Moshe,G. Achi Br,R. Basri. Prior knowledge driven multiscale segmentation of brain MRI. in international conference on Medical image computing and computer-assisted intervention. 2007: Springer-Verlag Berlin, Heidelberg

17. N. Ray,S.T. Acton,T. Altes,E.E. De Lange,J.R. Brookeman, Merging Parametric Active Contours within Homogeneous Image Regions for MRI-Based Lung Segmentation. IEEE Transactions on Medical Imaging, 2003. 22(2): p. 189-199.

18. C. Pluempitiwiriyawej,J. M. F. Moura,Y.L. Wu,C. Ho, STACS: new active contour scheme for cardiac MR image segmentation. IEEE Transactions on Medical Imaging, 2005. 24(5): p. 593-603.

19. B. Gilles,N. Magnenat-Thalmann, Musculoskeletal MRI segmentation using multi-resolution simplex meshes with medial representations. Medical Image Analysis, 2010. 14(3): p. 291-302.

20. H.P. Ng,K.C. Foong,S.H. Ong,J. Liu,P.S. Goh,W.L. Nowinski, A study on shape determinative slices for the masseter muscle. in International Conference of the IEEE Engineering in Medicine and Biology Society in conjunction with the Biennial Conference of the French Society of Biological and Medical Engineering. 2007. Lyon, France.

21. K. Held,E.R.Kops,B.J. Krause,W.M. Wells,R. Kikinis,H.W. Müller-Gärtner, Markov random field segmentation of brain MR images. IEEE Transactions On Medical Imaging, 1997. 16(6): p. 878-886.

22. T.N. Pappas,N.S. Jayant, An adaptive clustering algorithm for image segmentation. in ICASSP. 1989.

23. P.P. Wyatt,J.A. Noble, MAP MRF joint segmentation and registration of medical images. Medical Image Analysis, 2003. 7(4): p. 539-552.

24. N. Richard,M. Dojat,C. Garbay, Distributed Markovian segmentation: Application to MR brain scans. Pattern Recognition, 2007. 40(12): p. 3467-3480.

25. X. Liu,D.L. Langer,M.A. Haider,Y. Yang,M.N. Wernick,I.S. Yetik, Prostate cancer segmentation with simultaneous estimation of Markov random field parameters and class. IEEE Transactions On Medical Imaging, 2009. 28(6): p. 906-915.

26. Y. Zhang,M. Brady,S. Smith, Segmentation of brain MR images through a hidden Markov random field model and the expectation-maximization algorithm. IEEE Transactions on Medical Imaging, 2001. 20(1): p. 45-57.

27. K. Van Leemput,F. Maes,D. Vandermeulen,P. Suetens, Automated model-based tissue classification of MR images of the brain. IEEE Trans Med Imaging, 1999. 18(10): p. 897-908.

28. S.P. Awate,T. Tasdizen,N. Foster,R.T. Whitaker, Adaptive Markov modeling for mutual-information-based, unsupervised MRI brain-tissue classification. Medical Image Analysis, 2006. 10(5): p. 726-739.

29. A. Sotiras,N. Komodakis,G. Langs,N. Paragios. Atlas-based deformable mutual population segmentation. in IEEE International Symposium on Biomedical Imaging 2009.

30. T.R. Raviv,K. Van Leemput,W. M. Wells,P. Golland, Joint Segmentation of Image Ensembles via Latent Atlases, in Med Image Comput Comput Assist Interv (MICCAI). 2009. p. 272-280.

31. Z. Song,N.J. Tustison,B.B. Avants,J.C. Gee,. Adaptive graph cuts with tissue priors for brain MRI segmentation. in IEEE International Symposium on Biomedical Imaging. 2006. Piscataway.

32. R. Wolz,P. Aljabar,R.A. Heckemann,A. Hammers,D. Rueckert, Segmentation of Subcortical Structures and the Hippocampus in Brain MRI Using Graph-Cuts and Subject-Specific A-Priori Information. in IEEE International Symposium on Biomedical Imaging. 2009. Piscataway, NJ, USA.

33. F. Alexandre,R.F. El Sayed,T. Mascarenhas,R.M.N. Jorge,M.P. Parente,A.A. Fernandes, J.M.R.S. Tavares, 3D reconstruction of pelvic floor for numerical simulation purpose, Artigo em Conferência Internacional, 2008.

34. Y.H. Jiao,K.X. Zhao,Z.C. Wang,X.H. Qian,X. Wu,F.Y. Man,W. Lu,H.C. She, Magnetic resonance imaging of the extraocular muscles and corresponding cranial nerves in patients with special forms of strabismus. China Medical Journal (Engl). 2009. 122(24): p. 2998-3002.

35. P. Young,G. TABOR,T. Collins,J. Richterova,E. Dejuniat, Automating the generation of 3D finite element models based on medical imaging data Ultrasound, 2005. 44: p. 23–24.

36. G.G. Barbarino,M. Jabareen,J. Trzewik,A. Nkengne,G. Stamatas,E. Mazza, Development and Validation of a Three-Dimensional FiniteElement Model of the Face. Journal of Biomechanical Engineering, 2009. 131(4).

37. M.E. Farrugia,M.D Robson,L. Clover,P. Anslow,J. Newsom-Davis,R. Kennett,D. Hilton-Jones,P.M. Matthews,A. Vincent, MRI and clinical studies of

facial and bulbar muscle involvement in MuSK antibody-associated myasthenia gravis. Brain: A journal of neurology, 2006. 129(6): p. 1481-1492.

38. R. Olszewski,Y. Liu, T. Duprez, T. M. Xu and H. Reychler, Three-dimensional appearance of the lips muscles with three-dimensional isotropic MRI: in vivo study. International Journal Of Computer Assisted Radiology And Surgery, 2009. 4(4): p. 349-352.

39. 3D Slicer open-source software (Harvard Medical School, Boston, MA, USA).

40. H.P.W. Boom,P.H. van Spronsen,F.C. van Ginkel,R.A. van Schijndel,J.A. Castelijns, D.B. Tuinzing, A comparison of human jaw muscle cross-sectional area and volume in long- and short-face subjects, using MRI. Archives of Oral Biology, 2008. 53(3): p. 273-281.

41. V. Jurcak,J. Fripp,C. Engstrom,D Walker,O Salvado,S. Ourselin,S. Crozier, Atlas based automated segmentation of the quadratus lumborum muscle using non-rigid registration on magnetic resonance images of the thoracolumbar region, in ISBI. 2008: Paris. p. 113-116.

42. S. Klein,U.A. van der Heide,B.W. Raaymakers,A.N.T.J. Kotte,M. Staring,J.P.W. Pluim, Segmentation of the prostate in mr images by atlas matching, in ISBI. 2007: Arlington, VA. p. 1300 - 1303

43. J.H. Noble,F.M. Warrenb,R.F. Labadie,B. M. Dawant. Automatic Segmentation of the Facial Nerve and Chorda Tympani Using Image Registration and Statistical Priors. in SPIE. 2008.

44. H. Ng,S. Ong,S. Huang,J. Liu,K. Foong,P. Goh,W. Nowinski, Salient features useful for the accurate segmentation of masticatory muscles from minimum slices subsets of magnetic resonance images. Machine Vision and Applications, 2010. 21(4): p. 449-467.

45. H.P. Ng,J. Liu.,S. Huang,S.H. Ong,K.W.C. Foong,P.S. Goh,W.L. Nowinski, An improved shape determinative slice determination method for patient-specific modeling of facial anatomical structure. International Journal Of Computer Assisted Radiology And Surgery, 2008. 3(3): p. 221-230.

46. H.P. Ng,Q.M. Hu,S.H. Ong,K.W.C. Foong,P.S. Goh,J. Liu,W.L. Nowinski, Segmentation of the temporalis muscle from MR data. International Journal Of Computer Assisted Radiology And Surgery, 2007. 2(1): p. 19-30.

47. H.P. Ng,S.H. Ong,S. Huang,J. Liu, K.W.C. Foong,P.S. Goh,W.L. Nowinski, Salient features useful for the accurate segmentation of masticatory muscles from minimum slices subsets of magnetic resonance images, in Image Analysis and Interpretation. 2006: Denver, CO p. 208-212.

48. S. Z. Li, Markov random field modeling in computer vision. 1995: Springer-Verlag London, UK.

49. J. M. Hammersley,P. Clifford, Markov field on finite graphs and lattices. unpublished, 1971.

50. H. Derin,H. Elliott, Modeling and segmentation of noisy and textured images using Gibbs random fields. IEEE Transactions on Pattern Analysis and Machine Intelligence, 1987. 9(1): p. 39-55.

51. S. Kirkpatrick,C.D. Gellatt,M. P. Vecchi, Optimization by simulated annealing". Science, 1983. 220: p. 671-680.

52. C. F. J Wu, On the convergence properties of the EM algorithm. The Annals of Statistics, 1983. 11: p. 95-103.

53. B. Kim,J.L. Boes,K.A. Frey,C.R. Meyer, Mutual information for automated unwarping of rat brain autoradiographs NeuroImage, 1997. 5(1): p. 31-40.

54. J.P. Pluim,J.B. Maintz,M.A. Viergever, Mutual-information-based registration of medical images: a survey. IEEE Transactions on Medical Imaging, 2003. 22(8): p. 986-1004.

55. J.P. Thirion, Image matching as a diffusion process: an analogy with maxwell's demons. Medical Image Analysis, 1998. 2(3): p. 243-260.

56. F.H. Martini, Fundamentals of Anatomy and Physiology. 5 ed. 2001: Prentice Hall College Div.

57. Y.P. Yeoh,H. Ibrahim,N. Sia,P. Kong, Investigation on several methods to correct the intensity inhomogeneity in magnetic resonance images, in IEEE Conference on Innovative Technologies in Intelligent Systems and Industrial Applications 2008, IEEE. p. 55-59.

58. R.C. Gonzalez,R.E. Woods, Digital Image Processing. 2005: Prentice Hall.

59. Berlin Amira 3-D scientific visualization and data analysis package (ZIB, Germany; Indeed – Visual Concepts GmbH, Berlin, Germany; TGS Inc., San Diego, CA)

60. 3D Anatomy for Otolaryngology & Head & Neck Surgery. Available from: http://www.primalpictures.com/Otolaryngology-head-neck-surgery.aspx.

61. L.R. Dice, Measures of the Amount of Ecologic Association between Species. Ecology, 1945. 26: p. 297-302.